A STUDY OF LITHIUM-ION TRANSPORT IN PVDF-HFP BASED PIEZIOIONIC MEMBRANES WITH A BINARY CARBONATE SOLVENT MIX

by

Peter van den Doel

BACHELOR OF APPLIED SCIENCE

in

ELECTRICAL ENGINEERING

THE UNIVERSITY OF BRITISH COLUMBIA

(Vancouver)

April 2025

Supervised by Professor John Madden

Abstract

PVDF-HPF based piezoionic membranes utilizing LiTFSI electrolytes with carbonate solvents were fabricated and studied with a binary solvent mix. Lithium ion transport and solvation environment was investigated through electrochemical impedance spectroscopy and NMR spectroscopy. Utilizing propylene carbonate and dimethyl carbonate, a common lithium-ion battery solvent mix, ion transport was greatly enhanced in bulk solution, but not necessarily in the piezoionic membranes. Membranes containing 3M LiTFSI/PC:DMC showed promise due to uniquely high conductivity compared to other concentrations. Dimethyl carbonate appeared to dissolve and lower the structural integrity of PVDF-HFP, limiting the stretchability of the membranes. The volatility of dimethyl carbonate also increases the difficulty of rheological characterization and measurement of the piezoionic coefficient. Future work on binary solvent mixes for LiTFSI/PVDF-HFP based piezoionic sensors ought to focus on finding a thinning agent that is less miscible in PVDF-HFP, and encapsulation techniques to prevent solvent vapors from escaping and mitigate the toxicity of LiTFSI based membranes.

Table of Contents

.

Acknowledgments

I would like to thank Suhail and Callum for their support during my wrist fracture, helping me in the CAD design process. I would like to thank Adriana and Suhail, along with the rest of the Molecular Mechatronics folks, for their help in the lab and lending me a hand when I only had one. Thank you to Erfan, Bahar, Xin, and Daina for all their advice and experience. Thank you to Xin for providing me with my first chemical lab experience and allowing me to discover the joys of electrochemistry. Thank you to Dr. Dan Bizzotto and Dr. Előd Gyenge for teaching me the fundamentals of electrochemistry, and Dr. Joe Salfi and Dr. John Madden for teaching me the basics of charge transport. Thank you to Elizabeth for help with drawing figures. Thank you to Dr. Carl Michal for lending me your time and being so patient despite my mistakes, I learned a lot. Thank you to Yuta for answering my emails and providing me with advice on membrane fabrication. Finally, thank you to Dr. John Madden for providing me with a segue between electrical engineering and electrochemistry, giving me the unique opportunity to do this research. I felt way out of my depth, but your advice, inspiration, and feedback helped me with the literature review and finding a clear sense of direction. I hope I was able to provide insight into the questions you posed at the beginning of my thesis work.

Chapter 1: Introduction

1.1 The Piezoionic Effect and Motivation

Piezoionic sensors are a novel, soft, pressure sensing technology, offering lower stiffness and high current output compared to piezoelectric sensors, making them well suited for biomedical applications. The most accepted explanation for the piezoionic effect is that, as fluid is pushed through a polymer matrix under compression, anions and cations will move at different speeds, causing a net current flow. Woehling et al observed that, in an EMITFSI based piezoionic sensor, the direction of piezoionic current flow depends on whether the anion or cation has a higher diffusion constant, as measured through NMR spectroscopy.[1] Further work, by Dobashi et al, sought to model piezoionic sensors and investigate a variety of sensing modalities. Among the kinds of sensors investigated, the highest piezoionic coefficients, ranging from $1.4 * 10^{-8} V/Pa$ to $1.1 * 10^{-7} V/Pa$ were achieved by sensors utilizing an electrolyte of lithium bis(trifluoromethanesulfonyl)imide (LiTFSI) in propylene carbonate (PC), absorbed into a Poly(vinylidene fluoride-co-hexafluoropropylene) (PVDF-HFP) membrane. The authors attributed the high piezoionic coefficients to the high ionic mobility and permselectivity offered by the PVDF-HFP/LiTFSI/PC membrane system at high concentrations.[2],[3]

The use of PVDF-HFP membranes with carbonate-based electrolytes is reminiscent of common polymer electrolyte separator technology for lithium ion batteries.[4] The high hydrophobicity of PVDF-HFP precludes the use of an aqueous electrolyte, and thus a non-aqueous solvent like propylene carbonate is necessary.[5] The low solubility of most Lithium salts in carbonate-based electrolytes precludes the use of some lower cost lithium salts such as

lithium chloride, and thus one is left only with battery salts to work with. For propylene carbonate, LiTFSI is the only common lithium salt that offers a solubility above 1M, and thus it was the logical choice for a piezoionic sensor.

Dobashi et al proposed a model for the piezoionic strength, based on the idea of a polymer backbone hindering ion transport. The piezoionic coefficient indicates the relationship between the pressure on the sensor and open circuit potential (Equation 1.1.1).

$$\Delta V = -\frac{eCk}{\sigma\eta}\left[\frac{D_+}{D_{0+}} - \frac{D_-}{D_{0-}}\right]\Delta P = \alpha\Delta P \text{ EQ 1.1.1}$$

Where ΔV is the open circuit potential, e is the elementary charge, C is the concentration of the electrolyte, k is the permeability of the membrane, σ is the ionic conductivity, η is the electrolyte dynamic viscosity, D_+ and D_- are the diffusion constants of the cation and anion respectively in the membrane, D_{0+} and D_{0-} are the diffusion constants of the cation and anion respectively in the bulk electrolyte solution, ΔP is the applied pressure, and α is the piezoionic coefficient. Although the model proved inaccurate in concentrated PVDF-HFP, the model provides some insight into opportunities to improve the piezoionic coefficient. The piezoionic coefficient may be enhanced by a lower dynamic viscosity because ions can move to generate currents more easily, and it will be enhanced by a lower ionic conductivity because ion movement will induce a greater voltage. Piezoionic response will also be enhanced if a strong difference in diffusion coefficients can be maintained at higher concentrations. The polymer backbone does not hinder but instead helps transport at high concentrations in LiTFSI/PC/PVDF-HFP, so the model must be interpreted with caution.

Dobashi et al also developed a model for the short circuit current density generated by a membrane (Equation 1.1.2):

$$j_p = -eC\frac{k}{\eta}\left[\frac{D_+}{D_{0+}} - \frac{D_-}{D_{0-}}\right]\nabla P \text{ EQ 1.1.2}$$

Where j_p is the piezoionic current density and ∇P is a pressure gradient within the material. Short circuit performance may be enhanced by a higher diffusion coefficient, maintaining diffusion coefficients at higher concentrations, and lower viscosity. The output impedance of the device will also be lowered by increasing ionic conductivity. Once again, the short circuit current model must be interpreted with caution due to the assumption that the membrane hinders ion motion. Borrowing from the techniques of lithium-ion battery engineering, diffusion coefficients and ionic conductivity may be enhanced by lowering viscosity through the addition of a thinning agent to the electrolyte, such as dimethyl carbonate (DMC). There is room to find an optimal solvent mix, informed by a study on ion transport in these polymer membrane systems. Bulk electrolyte and membrane samples are studied using a binary solvent mix of 1:2 propylene carbonate(PC):dimethyl carbonate(DMC). Ionic conductivity and lithium diffusion coefficient measurements are performed to provide insight into the role of solvent thinners in these piezoionic sensors.

1.2 Background and Literature Review

1.2.1 Ion Transport in Electrolytes

Diffusion coefficients and charge carrier mobility may be related to one another for a fully dissociated solution using the Nernst Einstein relation (equation 1.2.1.1).

$$D = \frac{k_B T}{z_{eff} e} \mu \text{ EQ 1.2.1.1}$$

Where k_B is Boltzmann's constant, T is the temperature in kelvin, z_{eff} is the effective ionic valency, e is the elementary charge, and μ is the electrophoretic mobility of the ion. So long as ions are well solvated, z_{eff} will be equal to the ion's *valency*. Ionic conductivity per mole of a solution may be represented in terms of diffusion coefficients or mobilities by equation 1.2.1.2.

$$\Lambda = \frac{eF}{k_B T}\left(z_{eff+}^2 D_+ + z_{eff-}^2 D_-\right) = F z_{eff+} \mu_+ + F z_{eff-} \mu_- \text{ EQ 1.2.1.2}$$

Λ is the molar conductivity, F is faraday's constant, and plus and minus represent the cation and anion respectively. If either the anion or cation are mobile, it will contribute to the ionic conductivity, and this ionic conductivity alone will not reveal individual ion mobilities. [3] At higher concentrations or in less polar solvents, anions and cations do not dissociate fully and instead form pairs. [6] Fully solvated ions are the most mobile, with solvent separated pairs being less mobile, and directly contacting ions being even less mobile. Even if a solution is not saturated, the ions may still undergo incomplete dissociation without precipitating back into the solid phase. Typically, less mobile solvation structures form at high concentrations, and the Nernst Einstein relation holds true at low concentrations. [7] Although conductivity is related to diffusion coefficients, measured ionic conductivity will typically be less than what the Nernst Einstein equation predicts, with the difference being explained by net neutral ion pairs lowering z_{eff}. Ions may readily diffuse, but net neutral aggregates will not move in response to an electric field. The difference between conductivity predicted from diffusion constants and measured conductivity may serve as a metric for the degree of ion pairing. [3] Such analyses cannot be conducted in this work as diffusion coefficients were only measured for the cation.

Highly polar solvents, such as ethylene carbonate ($\epsilon_{EC} = 89.78$) or propylene carbonate ($\epsilon_{PC} = 64$), are employed to minimize the degree of ion pairing and effectively solvate ions. Although water is highly polar, it is electrochemically unstable and does not mix well with PVDF-HFP. The main issue faced by polar carbonate solvents is a relatively high viscosity ($\eta_{EC} = 2.56$ cP) [8], ($\eta_{PC} = 2.2cP$) [9] The effect of viscosity on diffusion coefficient can be approximated using the stokes Einstein equation for spherical solvation shells (EQ 1.2.1.3).

$$D = \frac{k_B T}{b\pi\eta r} \text{ EQ 1.2.1.3}$$

b is an empirical factor, and r is the effective radius of the solvated ion. Smaller solvation shells will have a smaller ionic radius allow for greater mobility. The spherical ion assumption does not hold in many systems, such as in propylene carbonate where a trigonal planar solvation shell ($Li(PC)_3$) may be exhibited according to some density functional theory (DFT) results. [10] Although approximate, the stokes Einstein relation correctly predicts that more viscous electrolytes experience lower diffusion constants. Viscosity typically increases with electrolyte concentration, compounding with the problem of ion pairing at high concentrations. [3] Battery engineers mitigate the issue of viscous electrolytes by mixing in thinner electrolytes such as diethyl carbonate ($\epsilon_{DEC} = 2.805, \eta_{DEC} = 0.3cP$), or dimethyl carbonate ($\epsilon_{DMC} = 3.107, \eta_{DMC} = 0.5$). Thinner solvents suffer from lower dielectric constants, and so generally a binary solvent mix is used with one highly polar solvent, and one low viscosity solvent. [9] These binary solvent mixes effectively combine the properties of the two solvents, with dielectric constant and viscosity taking on a value similar to a weighted average of the properties of the two solvents. [11] Although data was not found for LiTFSI in PC/DMC, Edimeh et al found that

conductivity of LiCLO4 in DMSO was strongly enhanced by adding around 0.4 to 0.7 volume fraction of DMC. DMSO is a highly polar solvent, and DMC is a low viscosity solvent (Figure 1.2.1.1). Results for other lithium salts and solvents must be interpreted with caution, but are useful for forming hypothesis. [12]

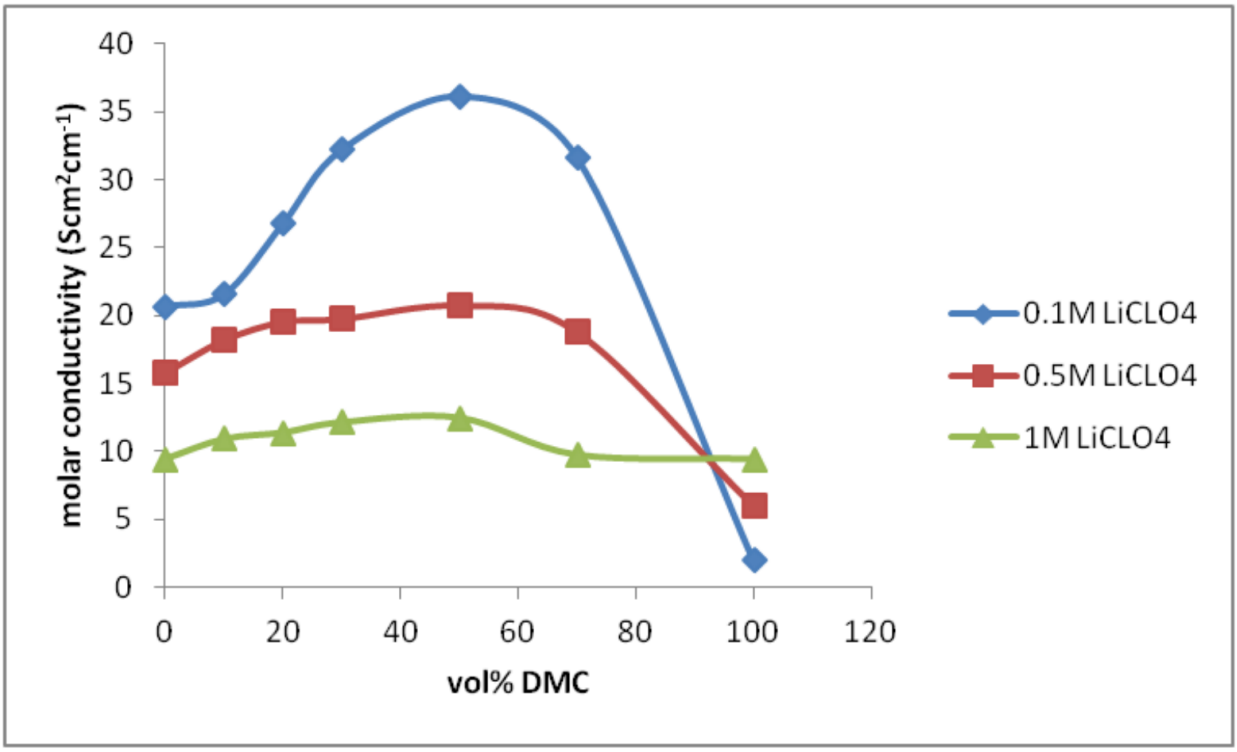

Fig 1.2.1.1: adapted from [12] Molar conductivity in a DMSO/DMC mix as a function of DMC composition for various concentrations. Conductivity is strongly enhanced for middle of the road solvent mixes, with the minimum at 0% DMC explained by high viscosity, and the minimum at 100% DMC explained by poor dissociation.

It was chosen to investigate membranes and electrolytes at a ratio of 1:2 PC:DMC to achieve the lowest possible viscosity without promoting too much ion pairing.

1.2.2 Ion Transport in PVDF-HFP

Dobashi et al investigated ionic conductivities and diffusion coefficients in LiTFSI/PC/PVDF-HFP systems for piezoionic sensors. It was found that the polymer enhances ion transport at high concentrations, and hinders transport at low concentrations (figure 1.2.2.1).

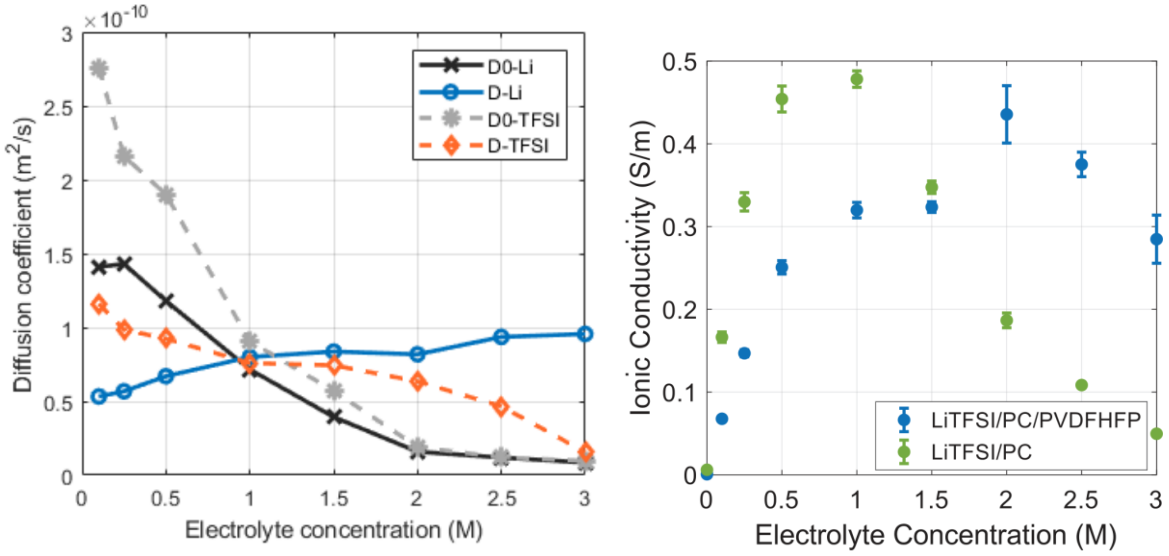

Figure 1.2.2.1: Adapted from Dobashi et al [2]

Right: D0 represents diffusion coefficients in bulk PC solution, while D represents diffusion coefficients in the polymer matrix. Both Li and TFSI show enhanced diffusion coefficients at high concentrations in the polymer matrix, with Li maintaining an especially high diffusion coefficient. Diffusion coefficients in the bulk solution monotonically decrease with concentration as expected.

Left: Ionic conductivity measurements show greater conductivity from the bulk solution at low concentrations, while the polymer shows greater conductivity at high concentrations, matching well with the trend in diffusion coefficients.

High TFSI mobilities and diffusion constants in bulk solutions have been explained in the past by rapid rotation between two conformers, with a small energy difference of 0.6kJ/mol, resulting in relatively little stable solvation shell formation and a small solvated ionic radius. [13]

The lower mobilities and diffusion constants of lithium ions have been explained through the formation of stable coordinated solvation complexes. Some literature argues that $Li(PC)_3$ is favored [14], and other literature argues that the larger $Li(PC)_4$ complex may be favored depending on the concentration. [15] The diffusion coefficient of Li and TFSI approach one another at high concentrations in bulk solution, indicating correlated diffusion and the formation of ion pairs.

The enhancement of LiTFSI conductivity in PVDF-HFP may potentially be attributed to the fluorophilicity of the polymer backbone groups preventing ion pairing. Fluorinated hydrocarbons are difficult to polarize, but can interact weakly with one another through London dispersion forces, referred to as fluorophilic interactions. Hernandez et al performed solvation studies on LiTFSI in fluorinated hydrocarbon solvents and found low solubility, but dissociation was promoted slightly by fluorophilic interactions between the fluorinated solvent and TFSI. [16] The increase in Li diffusion coefficients with concentration in PVDF-HFP suggests that TFSI may interact more strongly with the polymer as concentrations increase, shieling the lithium ions from pairing. Jie et al observed that a PVDF-HFP based electrolyte enhanced lithium transference numbers, attributing this effect to TFSI being partially immobilized by the polymer backbone. [17]

Ions solvated in solid state electrolytes typically show lower diffusion coefficients than bulk, but Dobashi et al observed PVDF-HFP enhanced TFSI diffusion coefficients compared to bulk. Weak interaction from the polymer backbone does not prevent TFSI from inhabiting a mobile liquid ionic atmosphere, but keeps the Li and TFSI in separate enough environments that

they interact less. Single phase diffusion was observed for both Li and TFSI in PVDF-HFP, so there is no evidence of a distinct polymer solvated and liquid solvated phase, but rather, one single phase. If there exists a second phase of Li or TFSI locked up in the polymer, it makes up a very small minority of ions. [3]

T1 decay measurements are another powerful way to probe the ionic atmosphere seen by lithium ions. Longer T1 times, on the order of 2-3 seconds, can indicate fast tumbling ions solvated by a low viscosity electrolyte. An increase in T1 will indicate more full dissociation into the liquid solvent. A decrease in T1, on the order of 50%, is characteristic of ion pairing or viscosity increases due to high concentration. A drastic reduction in T1, or two separate time constants, indicates ions bound up in a less mobile phase like a polymer backbone. [18] Based on the studies of Hernandez et al and Jie et al, lithium should not be solvated by the PVDF-HFP and only one T1 time constant should be seen.

It is hypothesized that the 1:2 PC:DMC solvent mix will show enhanced ionic conductivity in the bulk solution across all concentrations. 1:2 is a good ratio to enhance diffusion and conduction in solution, without encouraging too much ion pairing that may reduce permselectivity of the PVDF-HFP systems. The ion-solvent-polymer relationship in PVDF-HFP will only grow more complex as a binary solvent mix is used, but diffusion coefficient and ionic conductivity measurements can reveal how interactions vary with concentration. A fundamental study on LiTFSI in this solvent mix will add to the literature on binary solvent battery electrolytes. Studying transport in PVDF-HFP will shed light on the piezoionic properties of the material. Enhanced diffusion coefficients and conductivity at high concentrations would suggest

better piezoionic performance, both in open circuit and short circuit modes. Conductivity measurements are acquired at the exact same concentrations acquired by Dobashi et al, for the sake of easy comparison between results. Due to limited time on the NMR probe, only 4 samples were studied with NMR, looking at low and medium concentrations. Only the lithium ions are studied with NMR. Diffusion coefficient and T1 relaxation measurements will shed light on the ionic atmosphere seen by the lithium ions.

Chapter 2: Materials and Methods

Membranes and bulk solution were produced at LiTFSI concentrations of 0.1M, 0.25M, 0.5M, 1M, 1.5M, 2M, 2.5M and 3M to measure conductivity and compare with results from Dobashi et al and Petel. [2], [3] A more limited set of samples at only 0.1M and 1.5M were produced for lithium NMR measurements.

2.1 Liquid Ionic Conductivity Measurements

Ionic conductivity of liquid electrolyte samples was determined by measuring the resistance across a section of fluid with a simple and well-defined geometry. Assuming a prismatic section of electrolyte, the resistance R can be related to the ionic conductivity σ through EQ 2.1.1

$$R = \frac{L}{\sigma A} \quad \text{EQ 2.1.1}$$

L is the distance between the electrodes, and A is the area of the fluid section. EQ2.1.1 is applicable when there is a prismatic section of fluid between the electrodes, such as a cylindrical or rectangular section, and the electrodes contact the entire surface area of the fluid on each side. Deviations from the simple geometry will result in non-uniform equipotential surfaces and fringing fields, requiring finite element modeling to determine the relationship between conductivity and resistance. (Fig 2.1.1)

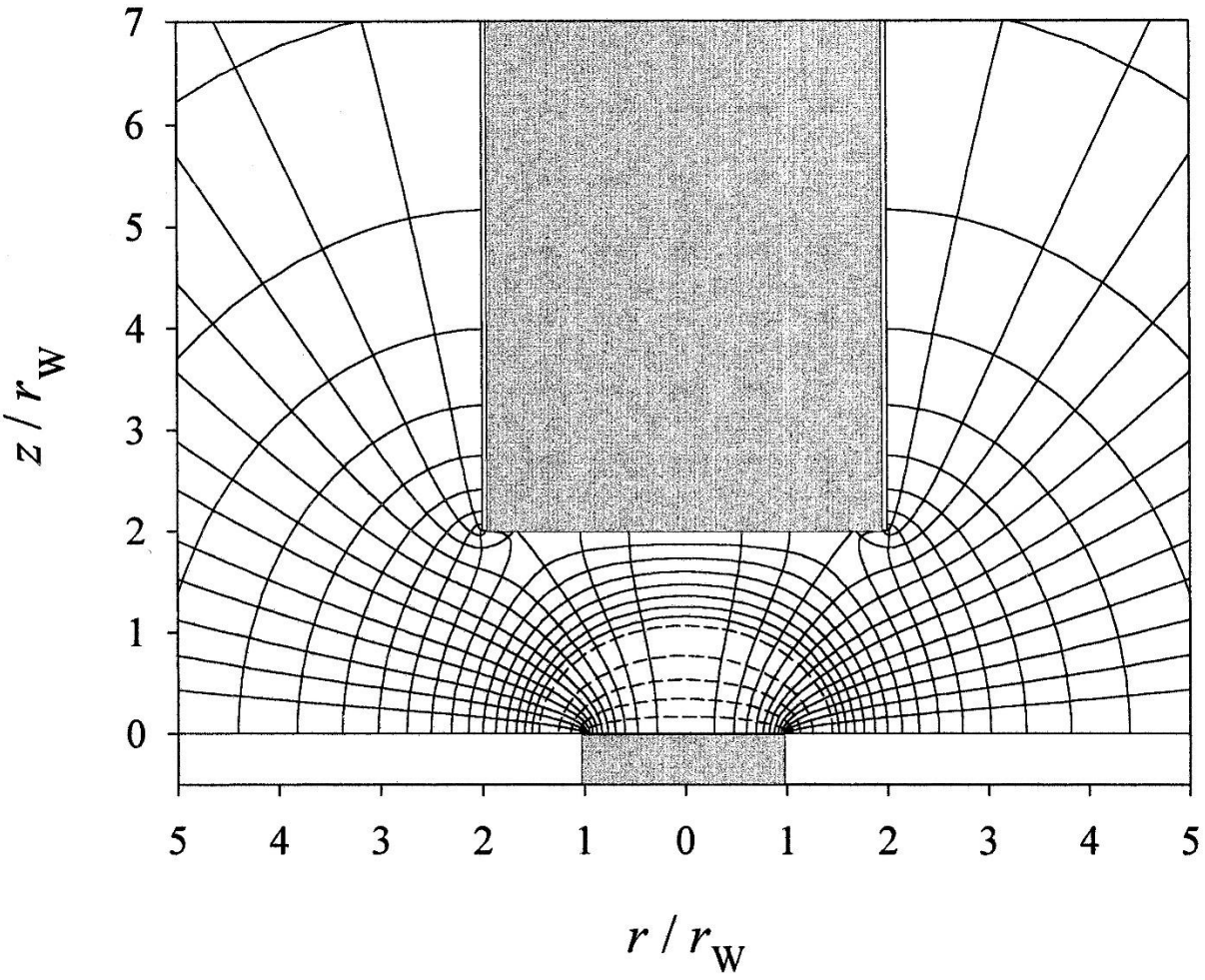

Figure 2.1.1: Adapted from [19]. An illustration of current and equipotential lines from a non-ideal electrode geometry, determined through finite element analysis.

The preferred method for measuring conductivity would have been a 4-point measurement cell utilizing two reference electrodes, but a cell of this nature requires a large amount of electrolyte and was impractical given the cost constraints of this research. Because PVDF-HFP is electrically insulating, a two-electrode setup with metal electrodes may be used so long as the double layer capacitances are accounted for in the impedance analysis.

A 3D-printed, cubic, 2 electrode cell was designed to measure conductivity with small fluid samples under 1mL Fig 2.1.2. The cell width matches the width of the electrodes, and slots were designed for the electrodes to sit in, keeping them flush against opposing walls. The size of the cell was chosen to be much larger than the wiggle room of the platinum electrodes in their slots, as this wiggle room represents an uncertainty in the inter electrode distance.

To standardize fluid height between experiments, small fill markers were incorporated into the 3D-printed cell. However, it was observed that the initial fill markers positioned the liquid level too low, allowing the fluid meniscus to occupy a significant fraction of the fluid surface area and distort the effective geometry. Additional fluid was added to ensure that the meniscus curvature remained small relative to the total fluid depth. Ideally, the entire cubic cell would be filled to maintain better geometry, but a smaller volume was chosen to reduce electrolyte use. A standard sample volume of 600 μL was chosen, resulting in a fluid depth of approximately 2.7 mm within the measurement cell. The meniscus that still exists will contribute some systematic error to measurement, increasing the measured resistance by a small proportion.

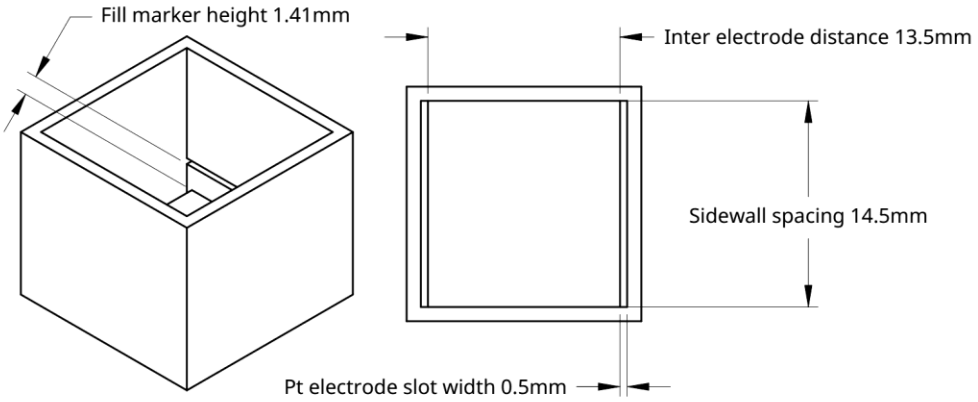

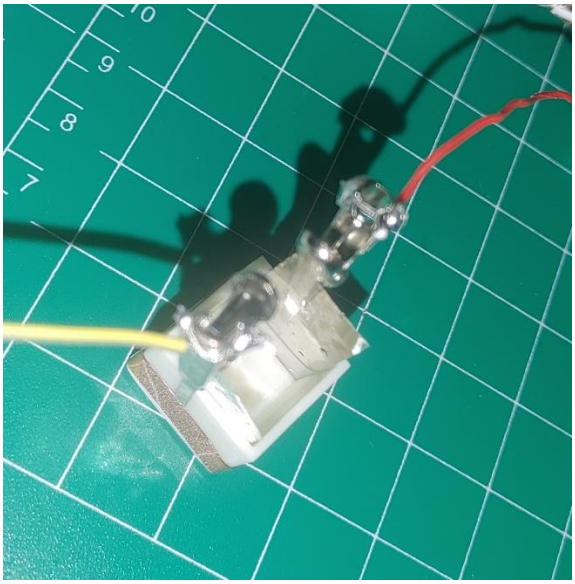

Figure 2.1.2:
Top: Mechanical drawings of ionic the conductivity cell design with relevant dimensions labeled. Note that the fill markers were disregarded during the use of the cell.
Bottom: Ionic conductivity cell with platinum electrodes sitting inside their slots, flush against the wall. Note that a meniscus can be seen in the liquid electrolyte.

Platinum foil electrodes were chosen as electrochemically inert blocking electrodes. Electrodes were prepared by first sonicating for 1 hour in deionized water, then sonicating for 1 hour in isopropyl alcohol to clean off residual adsorbates or dirt. A small open circuit potential of around ±20mV was observed, likely due to differing levels of dirt or adsorbates on the two electrodes, so voltage perturbations were applied relative to open the open circuit potential.

Due to the volatility of dimethyl carbonate, measurements had to be performed quickly to ensure an accurate result was acquired. After preparing each electrolyte sample, sets of two measurements were performed in quick succession. First, AC impedance spectroscopy was performed at 10mV RMS relative to open circuit from 0.1Hz to 32MHz in a two-electrode configuration, utilizing a Solartron SI 1260 impedance analyzer. This initial AC sweep took about 2 minutes. The resistance was taken as the lowest frequency zero crossing, where imaginary impedance reaches 0. A representative plot and analysis is given in figure 2.1.3. Second, the AC impedance was recorded at 10mV RMS relative to open circuit at 100KHz for 5 minutes. The standard deviation of real impedance in the final 2-minute window of this sweep was taken as being representative of the uncertainty in the resistance value. A representative plot is given in figure 2.1.4

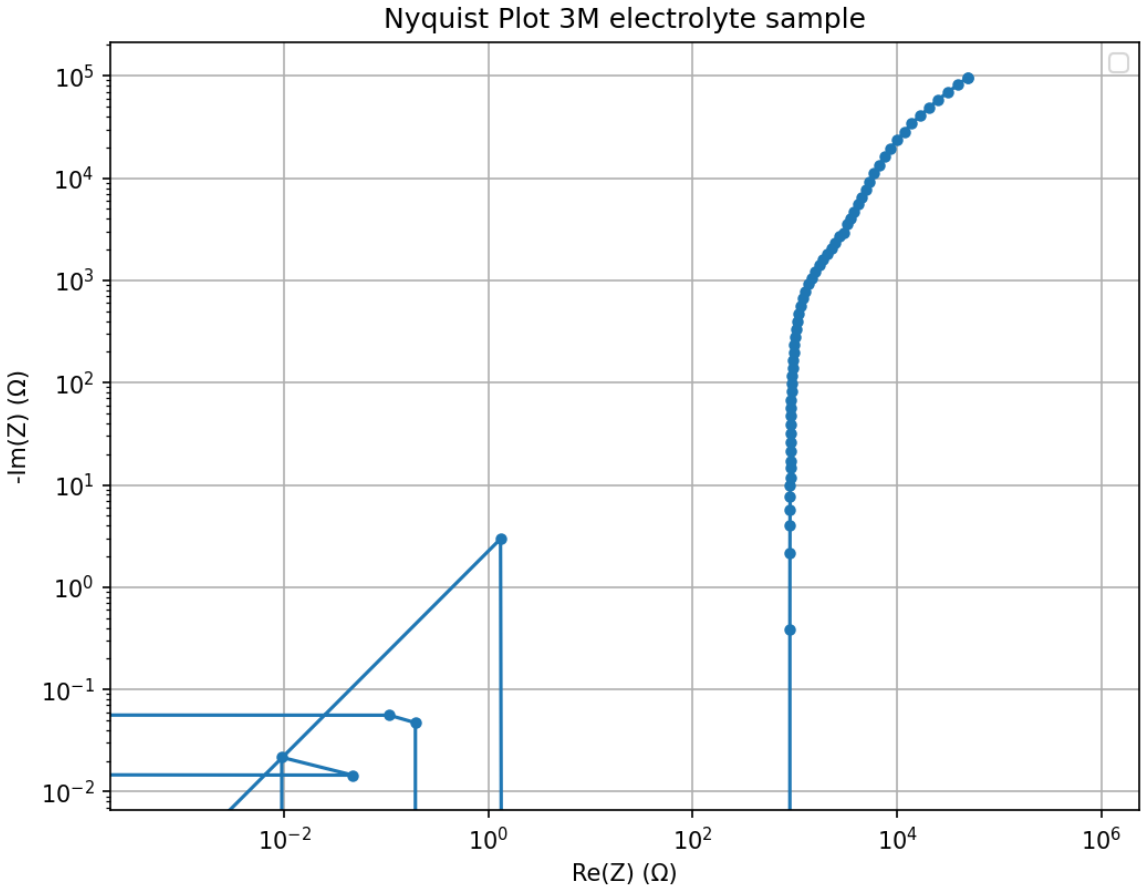

Figure 2.1.3: Log scale Nyquist plot of a 3M liquid electrolyte sample, the low impedance section to the left represents the region where the capacitance and inductance of the test setup create an effective short, independent of the electrochemical double layer capacitance. Note that inductive impedances appear negative and do not show up on this log scale plot. Towards the middle, the real impedance at the zero crossing represents the DC ionic resistance of the electrochemical system, and the double layer capacitance acts like a short circuit, while the impedance of the test setup acts like an open circuit. To the right, the impedance of the electrochemical double layers increases at low frequencies, with the real impedance also increasing due to the non-ideal nature of the double layer capacitance. Such a non-ideal capacitance would be modeled as a constant phase element.

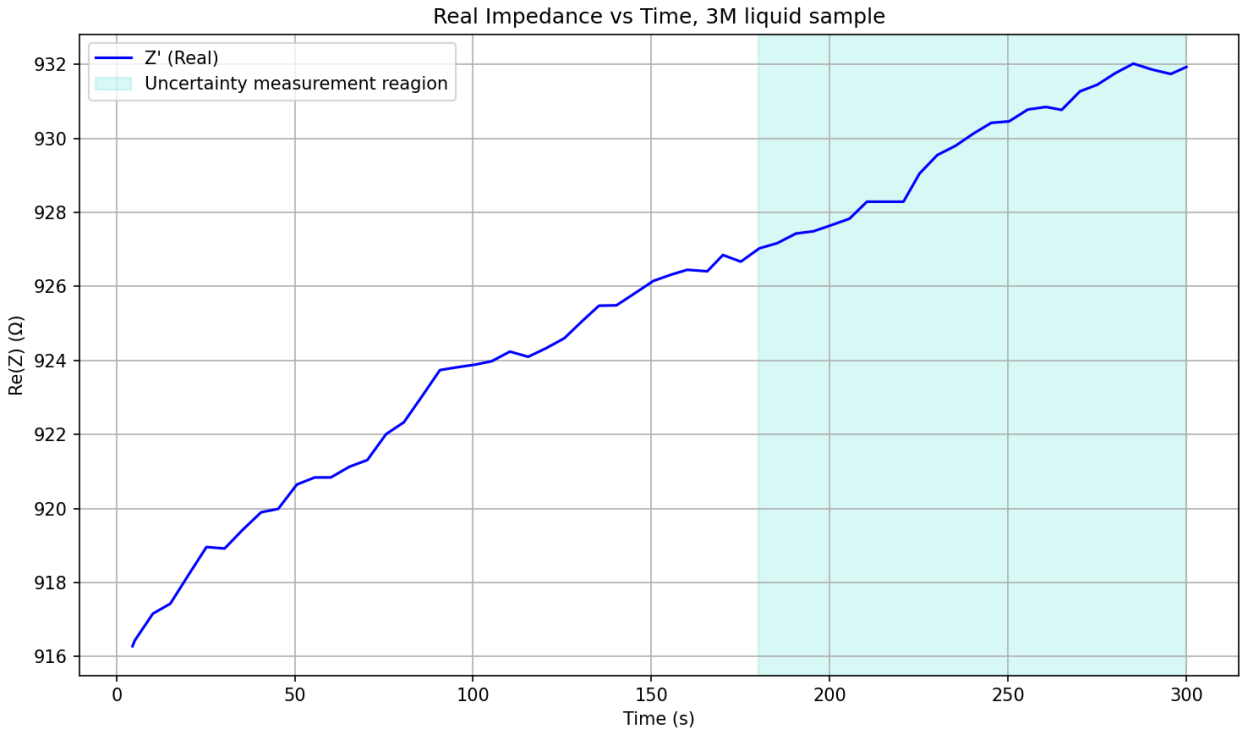

Figure 2.1.4: 100KHz real impedance vs time for 3M liquid electrolyte. The upward trend is due to evaporation of Dimethyl carbonate and reduction in effective contact area between the electrolyte and electrodes. The variation in the last two minutes of the curve is used as an estimate for the uncertainty in the resistance.

2.2 Membrane Fabrication

Two methods of membrane preparation were attempted. The first method proposed by Pu et al [5] produces dry, thin membranes, around $80\mu m$ thick, that must be soaked in electrolyte afterward. PVDF-HFP was dissolved in Acetone with water mixed in (give amounts), and the solutions were cast into small glass petri dishes to dry. The phase inversion involves mixing two mutually soluble chemicals (acetone and water), one of which the polymer is soluble in (acetone), and one of which the polymer is not soluble in (water). During the drying process, the acetone evaporates faster than the water. and the polymer de-mixes from the water in a

controlled manner, forming pores around pockets of water that then dry off. [20] Owing to a lack of a doctor blading machine, Pu et al's work could not be recreated and the technique failed to produce membranes with the desired uniformity and strength. Instead, membranes that were produced would curl during drying due to a lack of uniformity from the meniscus formed in the mold. Fabricated membranes would have some brittle nonporous regions, and some thin, porous regions. Membranes would soften and become flexible when soaked in electrolyte, but thinner regions would become fragile and fall apart when soaked in a PC:DMC mix. A thin film would form on the surface of the PC:DMC when mixed with these membranes, indicating that dimethyl carbonate may dissolve or break down the thin membranes.

The second technique used for fabricating membranes was proposed by Dobashi et al. [2] PVDF-HFP pellets were dissolved in acetone, and a LiTFSI propylene carbonate solution was mixed in with the dissolved polymer. Samples were placed in a mold with a perforated lid and allowed to dry slowly. As the acetone dries, pockets of electrolyte will form pores, and the membrane will be soft and swollen. Due to the lack of a doctor blading setup, achieving membrane uniformity was a challenge. Small petri dishes with a diameter of 40mm were purchased from Sigma Aldrich, with the intention of using them as molds. Small molds were chosen to ensure that, when fabricating samples with a variety of concentrations, minimal LiTFSI was used. It was discovered through experimentation and discussion with an author of Piezoionic Mechanoreceptors, that small molds produce non-uniform membranes due to the formation of a meniscus. Membranes with an acceptable surface uniformity were achieved by using a 10 by 15cm Pyrex container as a mold, where the larger surface area resulted in a meniscus that produced a more gradual curve on the fluid's surface (Figure 2.2.1). To avoid

using large amounts of electrolyte and running out of LiTFSI, it was chosen to fabricate membranes with bare PC inside and then soak them in electrolyte afterward. Membranes were cut out from the polymer sheet in discs of 12mm diameter, using a 3D printed cookie cutter. The cookie cutter was printed with a Formlasb Resin printer to achieve the resolution required to have a sharp cutting edge. The diameter of 12mm was chosen to exactly match the dimensions of the X2 Labs nutlocke cell to be used for ionic conductivity measurement (Figure 2.2.2). Fabricated membranes varied from 0.4mm thick in the center of the mold to 0.7mm thick towards the outside of the mold. Thickness variations within each membrane were around ±0.01mm to ±0.02mm in the center of the mold, with variability of around ±0.03mm to ±0.04mm towards the edges of the mold. The test results included in this work were performed on samples from the middle of the mold to minimize contact resistance from membrane inhomogeneity.

Figure 2.2.1:

Left: The fabricated PVDF-HFP/PC membrane sheet held in hand

Right: The fabricated PVDF-HFP/PC membrane in its glass mold. The perforated lid can be seen at the top. The slit shaped cuts were pieces taken out for NMR spectroscopy, and the circular holes were samples taken for impedance spectroscopy.

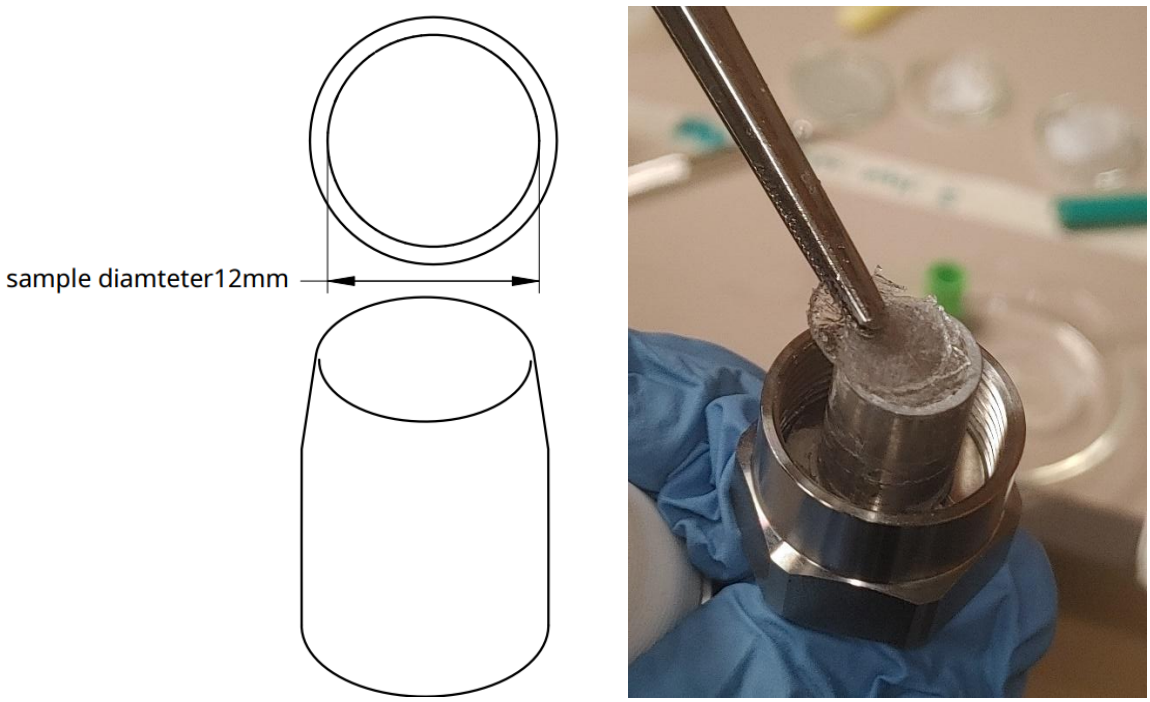

Figure 2.2.2
Left: mechanical drawing of the 3d printed cookie cutter
Right: An image of a damaged membrane sitting on the electrode of the nutlock cell. This membrane was damaged due to excessive force applied by the cell and was not included in the measurement data.

Due to the choice of a volatile cosolvent, dimethyl carbonate, Dobashi et al's procedure does not work because dimethyl carbonate evaporates along with the acetone. The fabrication procedure was modified to produce membranes with the desired concentration. Membranes were fabricated following Dobashi et al's procedure, but replacing the LiTFSI/PC electrolyte with the same volume of plain PC. Samples were cut out and weighed, and the propylene carbonate content was calculated based on the sample mass. To achieve a desired concentration with 1:2 PC:DMC solvent mix inside the sample, excess electrolyte was produced at 4 times the volume of PC inside the sample, and the sample was soaked in this excess electrolyte. Four times the

electrolyte volume was chosen to allow for a considerable excess volume that the sample could be dipped into, without needing to produce too much electrolyte. To achieve the desired solvent ratio, accounting for the volume of propylene carbonate inside the sample, the amount of solvent prepared for the soak was calculated according to equations 2.2.1 and 2.2.2.

$$V_{DMC} = \frac{5}{1.5} V_{PC\ inside} \text{ EQ 2.2.1}$$

$$V_{PC} = \frac{2}{3} V_{PC\ inside} \text{ EQ 2.2.2}$$

The concentration in the added electrolyte must be equal to the desired concentration multiplied by 1.25 so that the overall concentration ends up as desired after being diluted by the PC inside the membrane. After placing the required volume of electrolyte in a small scintillation vial lid, the membrane was soaked in the electrolyte for about 30 seconds, flipping it over multiple times to ensure all sides were fully wetted.

Membrane thicknesses were all measured with a Mitutoyo Absolute digital micrometer, accurate to $0.1\mu m$. Thickness was measured on four sections of the membrane, as illustrated in figure 2.2.3. The average of the thickness values was used as the membrane thickness, and the standard deviation of the four values was used as the uncertainty in thickness. Thickness variation may introduce systematic error in measurements, such as changes in contact resistance.

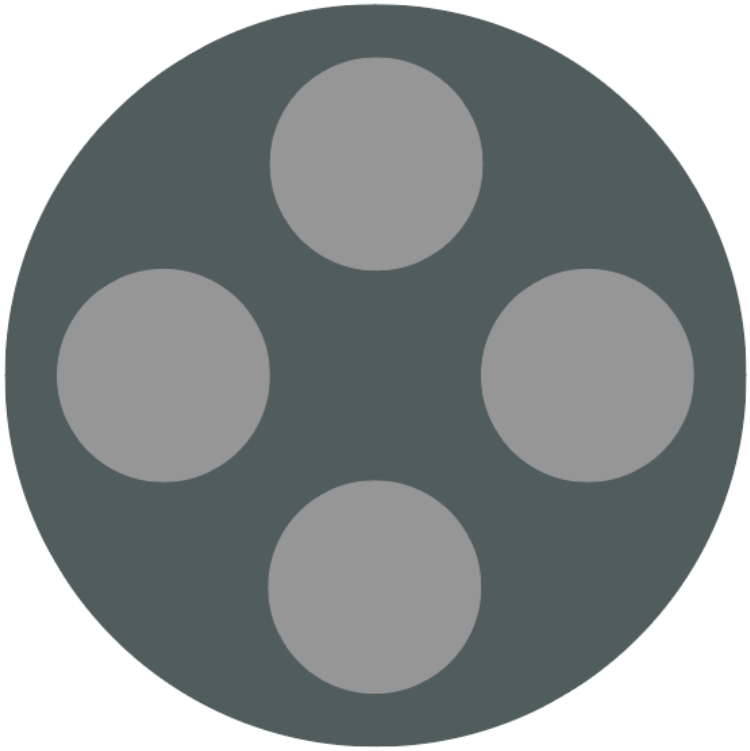

Figure 2.2.3: Credit to Elizabeth Lim for the drawing. Thickness was measured around the 4 edges of the membrane. Measurements were averaged to get the membrane thickness, and the standard deviation was used to determine uncertainty in the thickness.

Membranes expanded upon soaking in the electrolyte. Although it was not possible to measure the expansion of every sample due to the rapid drying of the DMC, one membrane was weighed before and after soaking, and another membrane had its thickness measured before and after soaking. From these results it was determined that membrane thickness swells 17.27%, and the

mass of electrolyte in the sample increases by 32.43%, with the overall mass of the sample increasing by 24.23%. For the sake of simplicity, changes in membrane diameter after soaking appeared negligible and were not accounted for.

2.3 Membrane Ionic Conductivity Measurements

Ionic conductivity of the membranes was measured with impedance spectroscopy. Due to the simple disc geometry of the membrane, the surface area and thickness of the membranes can be used to calculate the conductance according to equation 2.1.1. Measured membrane thicknesses were all multiplied by a 1.1727 correction factor to account for swelling from absorbed electrolyte. PVDF-HFP membranes were cut out into discs and prepared for measurement in an X2 lab nutlock type cell. The components of the cell were cleaned in preparation for measurements. First, the surfaces of the electrodes were cleaned with soap and water. Then, the components of the cell were sonicated for an hour in deionized water, then in isopropyl alcohol. Due to the small size of the membrane, it is important to ensure that dimethyl carbonate does not evaporate out of the cell during measurement. This was tested by placing a membrane in the cell and putting it on a scale accurate to 0.1mg. After 10 minutes, no change in mass was observed. The nutlock cell suffered from the issue that, without a torque wrench, a standard pressure could not be applied on all samples. Measurement stability was determined by pressing the membranes into the cell and measuring the real impedance at 100KHz for ten minutes. Once samples were pressed into the cell, the resistance reduced for a period of a few minutes before settling or drifting differently. It was hypothesized that this drift may be due to evaporation of dimethyl carbonate or dimethyl carbonate breaking down the polymer structure of the membrane. As was observed before, thin membranes soaked in dimethyl carbonate became

fragile and appeared to dissolve. A sample soaked in 0.1M propylene carbonate electrolyte was used as a control, and it exhibited the same drift **(**Figure 2.3.1). It is believed that the drift in the sample resistance is due to membrane slowly squishing and undergoing viscoelastic deformation under the pressure applied between the nutlock cell electrodes.

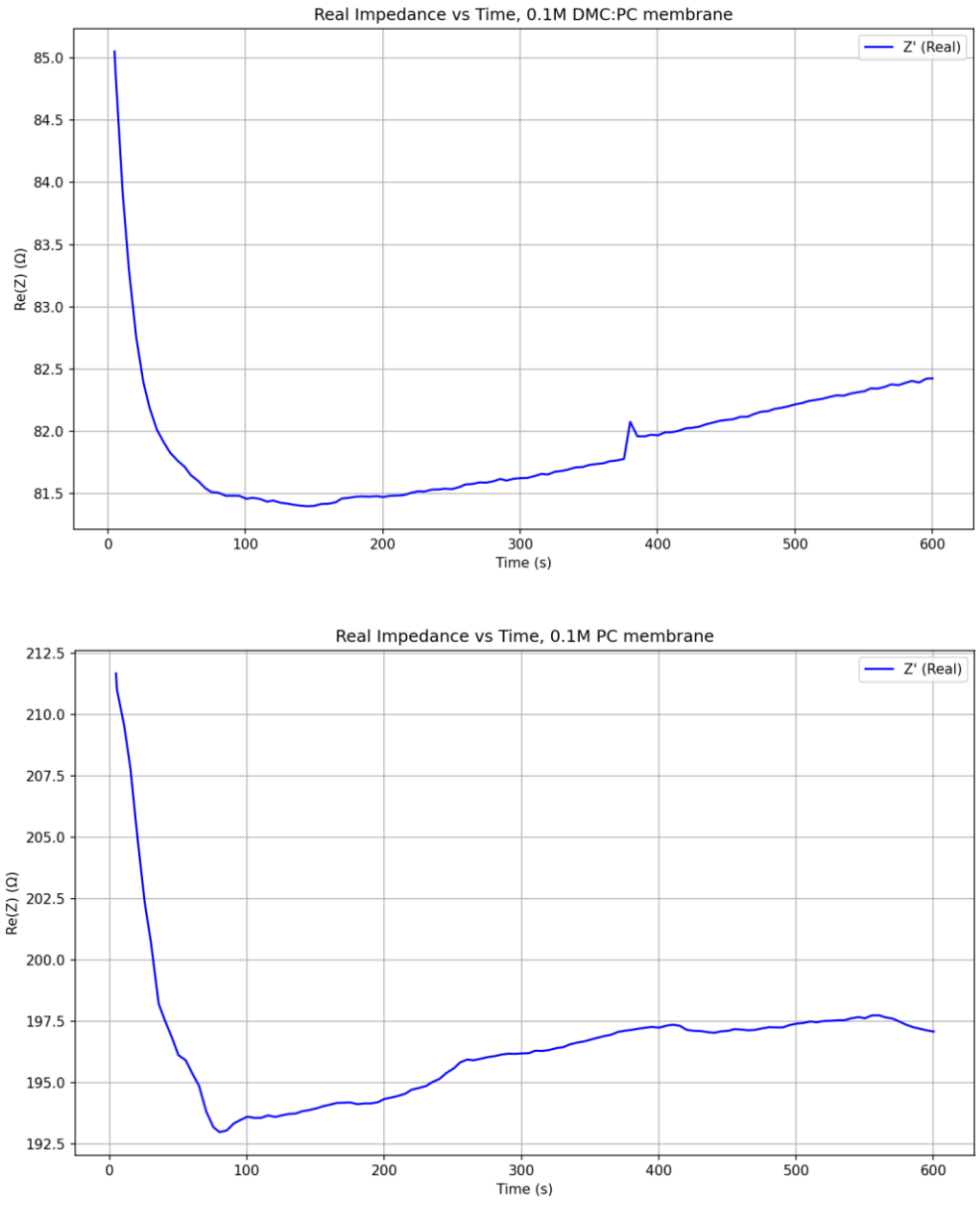

Figure 2.3.1: Resistance over time upon pressing the membrane into the nutlock cell. Membrane with a DMC:PC solvent mix shown on the top, membrane with a PC solvent shown at the bottom. The two samples have different thicknesses and surface inhomogeneities, but both show a clear drift in measured resistance, likely due to viscoelastic deformation under the pressure of the cell.

Better impedance stability was observed when the membranes were pressed into stainless steel coin cells as opposed to the nutlock cell. Coin cell casings, spacers, springs, and a press from Dongguan Zhik were all used. The coin cells were each pressed to 100psi for ten seconds. Coin cells placed on the scale showed no observed change in mass over ten minutes, indicating that DMC was not evaporating out of the samples. Each coin cell was first tested for stability by measuring the resistance at 100KHz for 5 minutes. If the stability was satisfactory, the resistance was measured by performing AC impedance spectroscopy from 32MHz to 0.1Hz at 10mV RMS relative to open circuit potential. EIS Measurements from a representative coin cell pressed sample are shown in Figure 2.3.2.

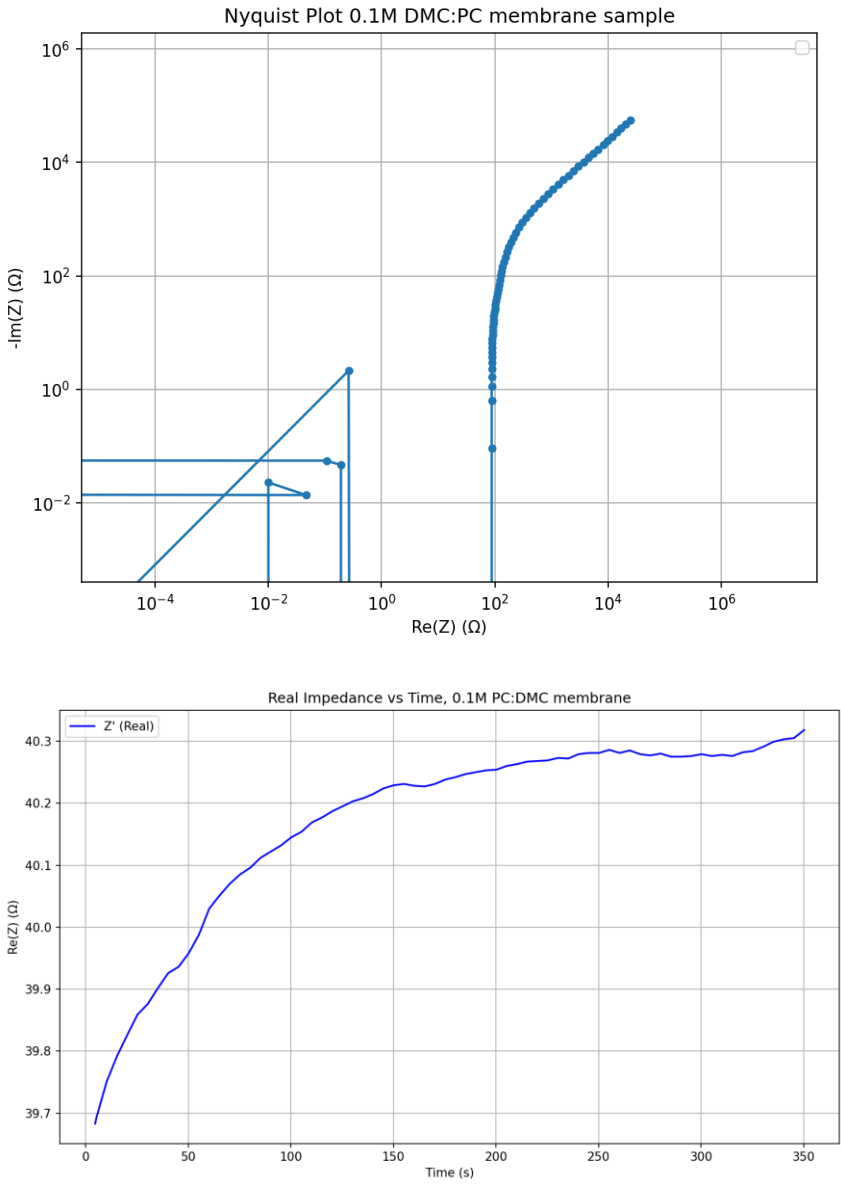

Figure 2.3.2:
Top: Log scale Nyquist plot of a 0.1M polymer sample, the different regions may be interpreted in the exact same way as was done for the Nyquist plot of the liquid measurements.
Bottom: Plot of 100KHz membrane impedance over 5 minutes, the measured drift is considerably smaller than what was measured in the nutlock type cell. It is speculated that the slight drift comes from contact resistance changes due to deformation of the electrodes that the membrane is pressed between.

2.4 NMR Measurements

Li^7 NMR spectroscopy was performed on bulk electrolyte and membrane samples to measure lithium diffusion coefficients and T1 spin lattice decay times. Measurements were carried out with the help of the UBC solid state NMR group on a custom-built NMR probe. More information on the design of this probe can be found in [21]. More information about NMR spectroscopy and the pulse sequences used can be found in appendix A.

2.4.1 Acquiring Diffusion Coefficients with PFG-STE NMR

Pulsed field gradient stimulated echo (PFG-STE) is an NMR spectroscopy sequence that can be used to measure the diffusion coefficients of ions in viscous electrolytes. The signal strength received from performing the sequence follows the Stejskal and Tanner equation (EQ 2.4.1.1).

$$\ln(S) = \ln\left(S_{no\ gradient}\right) - D\gamma^2\delta^2 g^2\left(\Delta - \frac{\delta}{3}\right) \quad \text{EQ 2.4.1.1}$$

Where γ is the gyromagnetic ratio of the nucleus of interest, δ is the duration of the gradient field pulse, g is the strength of the magnetic field gradient, and Δ is the diffusion time. $\delta, g,$ and Δ are all user defined parameters of the sequence, and one can acquire the diffusion coefficient by varying any of them, and fitting the data to acquire D. Varying Δ is problematic as different sequences will experience different amounts of T1 decay and samples must be normalized relative to this to fit the ST equation. Varying δ is problematic due to the somewhat convoluted dependence of the signal on δ. For measuring the diffusion coefficient of lithium, it was chosen to vary the gradient strength g, and a linear plot of $\ln(S)$ against g^2 was curvefit. The slope represents $-D\gamma_{Li}^2\left(\Delta - \frac{\delta}{3}\right)$ which can be used to acquire the diffusion coefficients. The y intercept

represents ln ($S_{no\ gradient}$) which is an unpredictable function of the sample, test setup, and pulse sequence. If a clean single diffusion constant fit is achieved, it indicates that the ion being studied exists in only one kind of ionic environment. [3] A representative linear and nonlinear fit are shown below in figure 2.4.1.1.

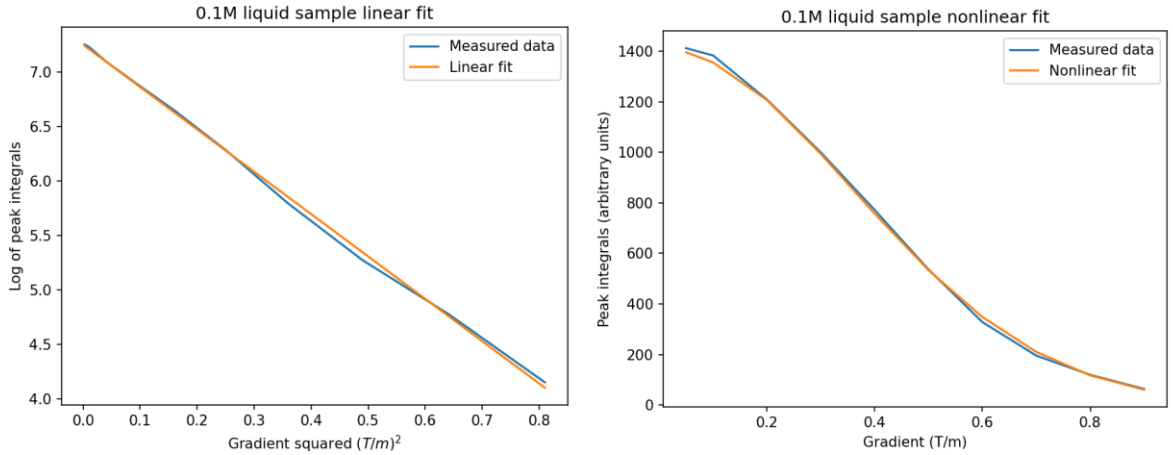

Fig 2.4.1.1. Linear and nonlinear fits of PFG–STE data from a 0.1M LiTFSI 1:2 PC:DMC sample. The good fit quality indicates single phase diffusion.

2.4.2 T1 Inversion Recovery Measurements

T1 relaxation time constants can be measured using a sequence called T1 inversion recovery, illustrated in figure 2.4.2.1.

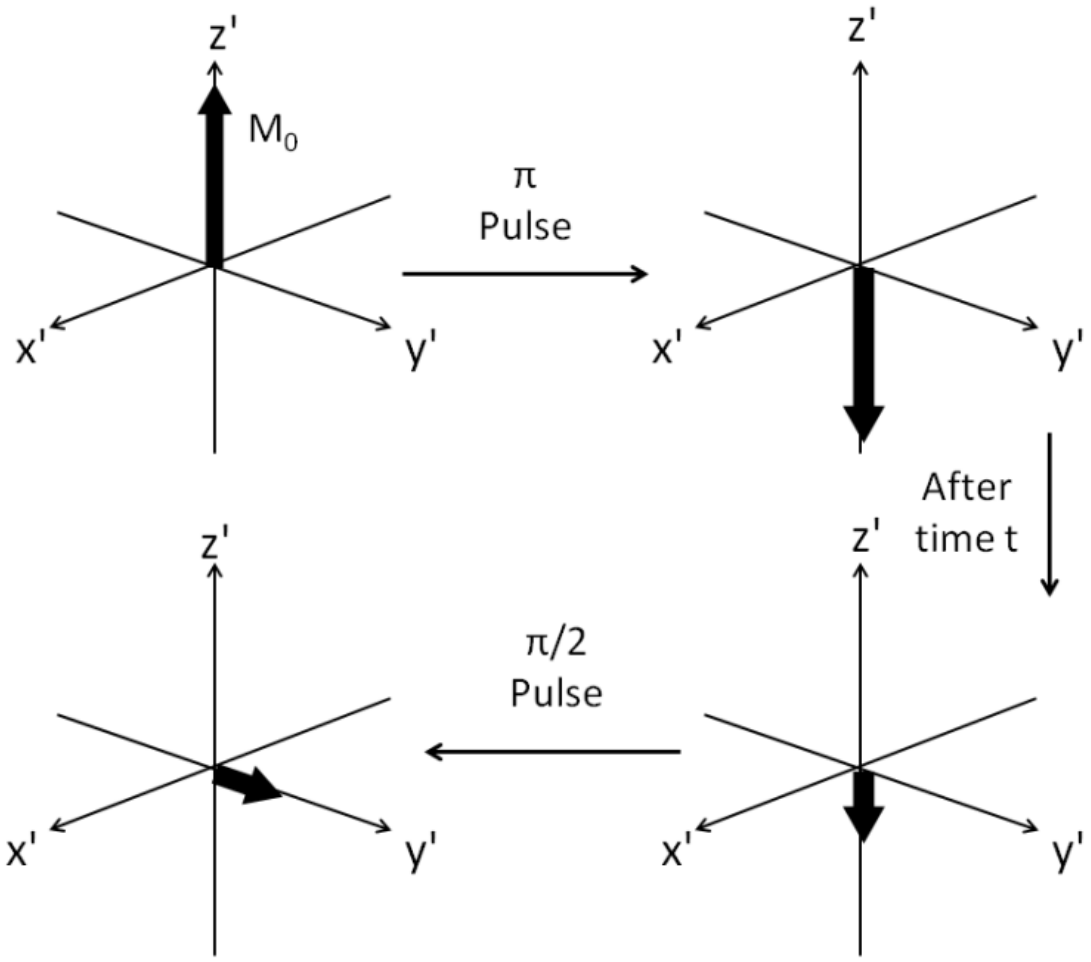

Figure 2.4.2.1: adapted from [18]

First: the sample is hit with a 180° pulse to begin the process of T1 decay

Second: T1 decay is allowed to occur for given period

Third: A standard spin echo sequence is performed to measure the echo signal strength.

In T1 inversion recovery, the sample is hit with a 180° pulse to orient the spin magnetization antiparallel to the magnetic field. After a certain amount of time, the sample is hit with a 90° pulse and a spin echo sequence is performed to measure the response. By varying the amount of time between the initial 180° pulse and the 90° pulse, one sees an exponential decay in echo strength indicative of T1 decay following equation 2.4.2.1.

$$S = A - B * e^{-\frac{t}{T1}}$$ EQ 2.4.2.1

A and B are fitting parameters, and t is the amount of T1 decay time in the pulse sequence. One will vary the decay time and observe the exponential change in received signal. If a clean single exponential decay is observed, it indicates that the ion being studied is only inhabiting one single phase. [18] A representative T1 inversion recovery curve fit is shown in figure 2.4.2.2.

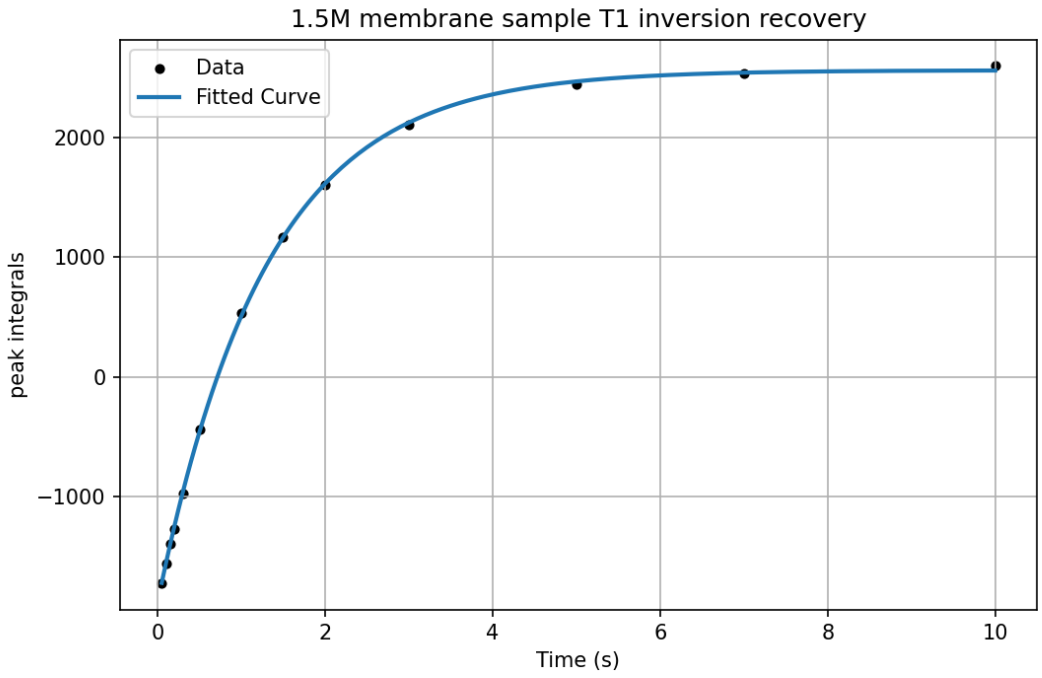

Figure 2.4.2.2: T1 decay profile and curve fit from inversion recovery sequence for a 1.5M membrane sample. The clean fit indicates all ions inhabiting a similar ionic atmosphere.

Chapter 3: Results and Discussion

Ionic resistance values were acquired at a variety of concentrations in bulk electrolyte and polymer samples, mimicking the concentration sweep performed by Dobashi et al. Ionic conductivities are extracted from these values using best estimates of membrane and fluid geometries. NMR diffusion and T1 measurements are interpreted and compared against results from Dobashi et al and Petel. Issues with data interpretation are discussed, and explanations are proposed for anomalous findings. Open questions remain, and a clear direction is provided for future research.

3.1 EIS Data Analysis

Before presenting the results of the ionic conductivity analysis, it is important to define how concentrations will be measured. Molarity is the number of moles per unit volume of solution, but solutions will expand if large amounts of solute are dissolved. When calculating molarity of highly concentrated solutions, electrolyte density must be used to correct for expansion. It is often customary to quantify large concentrations in molality (moles of solute per kilogram of solvent), or mole fraction (moles of solute per mole of solvent). While Dobashi et al and Petel measured concentrations in molars, they did not measure volume changes and thus their concentrations were approximate. Through the course of this research, it was observed that a prepared 3M solution of LiTFSI in 1:2 PC:DMC expanded by about 25% when solute was added. For ease of presentation, but also accuracy, concentrations will be represented in both molars and mole fractions, with the understanding that molars refers to moles of solute per liter of bare solvent.

3.1.1 Ionic Conductivity Analysis

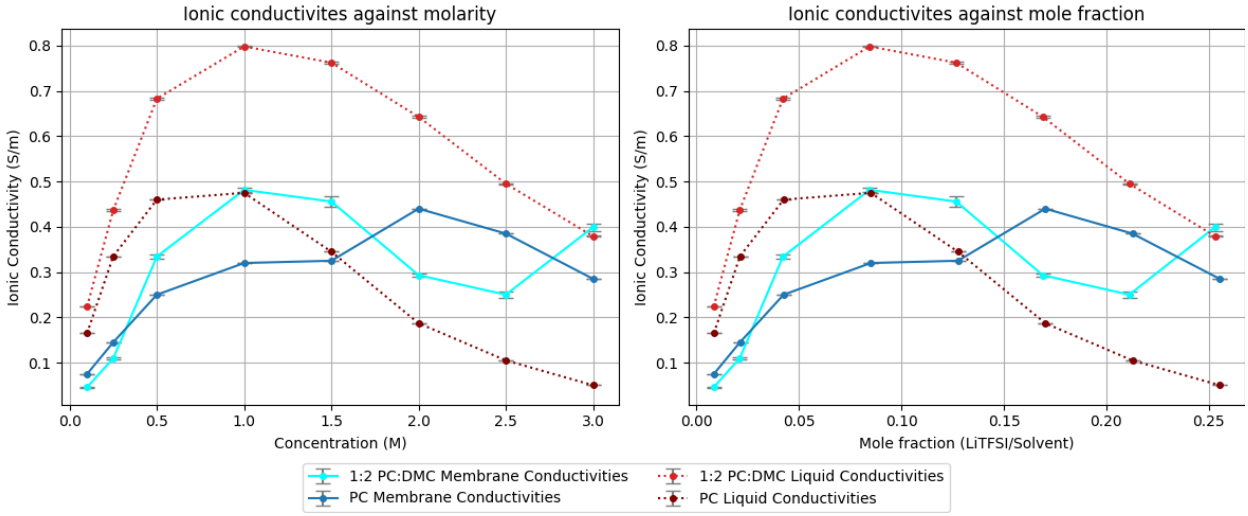

Figure 3.1.1.1: Ionic conductivities against concentration (left figure) and against mole fraction (right figure), of samples acquired in this work with 1:2 PC:DMC, compared with conductivities acquired by Dobashi et al in PC. Liquid samples are shown with red dashed lines, while membrane samples are shown with blue solid lines. Samples with PC:DMC have lighter colors while samples with PC have darker colors. Liquid samples show the characteristic increase in conductivity, until a peak, both around 1M (or 0.1 mole fraction). Swollen membranes show irregular conductivity relationships, increasing with concentration until around 1M (or 0.8 mole fraction), and then fluctuating up and down.

Ionic conductivities show a clear enhancement from the addition of DMC to the solvent mix. Liquid conductivities vary similarly with concentration, with a peak around 1M (or 0.8 mole fraction) followed by a decline. PC:DMC samples maintain very high conductivity at high concentrations, showing about a factor 8 enhancement compared to plain PC at 3M (or 0.25 mole fraction). Reductions in viscosity may potentially explain such enhancements, as Dobashi et al observed nonlinearly increasing viscosity with LiTFSI concentration in PC, providing a strong

motivation for thinning out the solvent (Figure 3.1.1.2).

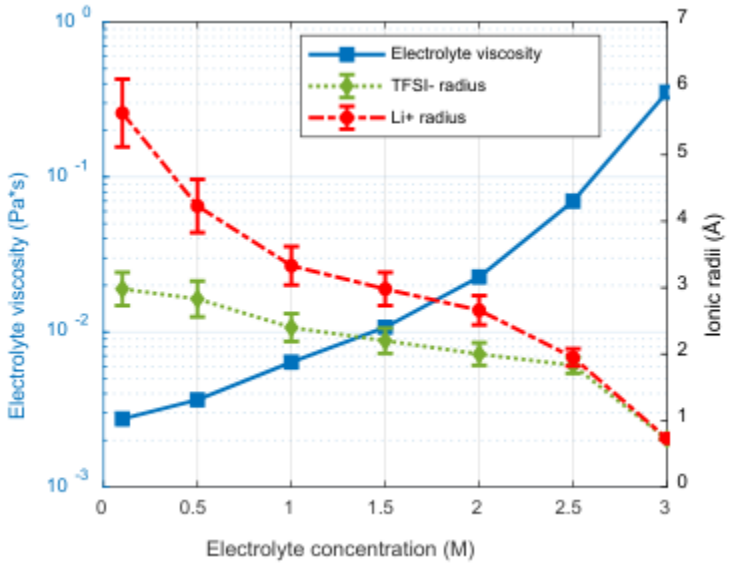

Figure 3.1.1.2: adapted from Dobashi et al. [2] LiTFSI/PC dynamic viscosity vs concentration. Viscosity increases nonlinearly with concentration, emphasizing the importance of a thinner solvent for maintaining ionic mobility. Ionic radii, estimated from NMR and viscosity data, become unrealistically low at high concentrations, demonstrating the limited accuracy of the Stokes Einstein relation (EQ 1.2.1.1).

An explanation is proposed for the observed inaccuracy in ionic radius estimates, raised during discussions with Dr. Madden. DFT analysis by Shi et al suggest that, as concentration increases above 2M, lithium solvation shells in propylene carbonate transition from a larger tetrahedral structure $(Li(PC)_4)$ to smaller planar structures $(Li(PC)_3, Li(PC)_2)$ [15]. The stokes Einstein equation (EQ 1.2.1.1) indicates that if viscosity grows faster than the diffusion coefficient shrinks, the ionic radius must be shrinking to make up the difference. DFT modeling indicates that ionic radii do shrink to an extent, but the estimates are far too small. The Stokes Einstein equation also assumes a spherical non deformable solvation shell, which is less valid for planar structures at high concentrations. The Stokes Einstein equation may be modified to better

suit modeling lithium ions by changing the b factor, but it is based on faulty assumptions at higher concentrations. Further work should investigate electrolyte viscosity with the PC:DMC solvent mix, to confirm the role of viscosity in the conductivity enhancement seen at medium to high concentrations.

The PVDF-HFP membrane conductivities are not necessarily enhanced by dimethyl carbonate, but which kind of membrane is more conductive depends on LiTFSI concentration. The back and forth relationship between the membrane conductivities is indicative of a very complex solvation relationship, with ion pairing or solvation structure shifting across the concentration sweep. The more complex relationship compared to the bulk electrolyte indicates a clear effect of the PVDF-HFP on solvation shell formation. The PC:DMC membrane hardly ever exceeds the conductivity of bulk PC:DMC. At high concentrations, the environment of both LiTFSI/PC/PVDF-HFP and LiTFSI/PC:DMC/PVDF-HFP membranes is generally better for mobility than that of the viscous PC solution, but worse than that of the battery style PC:DMC electrolyte. The mixed solvent membranes exhibit high conductivity at 3M (or 0.25 mole fraction), matching the conductivity of bulk PC:DMC solution. The sudden shift seemed anomalous, so a second 3M membrane was fabricated, yielding similar results. The 3M PC:DMC membrane may represent a goldilocks zone for the strongest piezoionic response, and yet higher concentrations may continue to show good conductivity.

3.1.2 Error Introduced from Differences in Membrane Fabrication

Conductivity differences between both membrane types must be interpreted with caution, as the fabrication procedures differed fundamentally. Dobashi et al dried their membranes with LiTFSI inside, but LiTFSI was added to the PC:DMC membranes by soaking them in electrolyte, effectively saturating all the pores. Soaking the membranes after fabrication led to a measured increase in electrolyte content of 32.43% by mass, and thickness swelled by 17.27%. Increased electrolyte content may cause liquid pockets inside the polymer to be larger, and reduce the relative effect of the polymer backbone on solvation. LiTFSI/PC:DMC soaked membranes may exhibit higher ionic conductivity than if they had the smaller electrolyte content of Dobashi et al's LiTFSI/PC membranes.

Electrolyte saturation and precipitation may confound differences between the two membrane fabrication techniques. Xin et al observed that LiTFSI saturates at 0.197 mole fraction in DMC, and 0.183 mole fraction in PC, and binary mixtures of solvents show solubilities in between the two [22]. The 2.5M and 3M electrolytes are saturated for both PC, and a PC:DMC mix. The liquid electrolytes were well mixed right before conductivity measurement, and PC:DMC membranes were measured immediately after soaking, allowing very little time for precipitation to occur. Dobashi et al fabricated their membranes by adding electrolyte to the polymer stock and allowing them to dry over 2 days. Unless the PVDF-HFP enhanced the saturation point of the electrolyte in its pores, there may have been some LiTFSI precipitation while drying. LiTFSI/PC membranes may have shown a lower ionic conductivity than if they were fabricated without a long drying process.

Structural changes may have occurred in the PVDF-HFP upon soaking in the PC:DMC solution. It was observed that, when mixing very thin membranes in PC:DMC, they lost their structural integrity and fell apart. A film would form on the liquid surface as though the membranes were dissolving. Such a film was not observed in the thicker samples that were measured, but fragility was. Samples prepared for NMR were easily damaged when removing them from the NMR tubes, having the consistency of a firm gel that would become damaged under too much force. Test samples exposed to PC solutions did not lose robustness. Rheological studies would help to indicate if the membranes have the required strength to function as piezoionic sensors, although the volatility of DMC would make such studies difficult. The initial literature review did not focus on the solubility of PVDF-HFP in the electrolyte, but it appears to have had a strong influence on the mechanical properties of the membranes. Employing Floury Huggins theory, Kim determined that PVDF-HFP is much more soluble in DMC than in PC, with interaction parameters of $\chi_{12DMC} = 83.07K/T$ and $\chi_{12PC} = 107.59K/T$, where a lower interaction parameter indicates greater solubility between a polymer and a solvent. [23]
Given the complex solvation environment in PVDF-HFP, it is hard to say whether structural changes induced by DMC hinder or enhance ion mobilities. Structural changes to the PVDF-HFP may reduce mobility by collapsing the pore structures, creating more hinderance for the ions. DMC solvating PVDF-HFP may block fluorophilic interaction sites, reducing the interactions that suppress ion pairing at high concentrations. It is also possible that the interaction of DMC with the polymer may increase pore size, or change solvation structure in a way that favours mobility.

3.1.3 Molar Conductivity Analysis

Molar conductivities provide a direct measure of overall ionic mobility, irrespective of concentration (Equation 1.2.1.2). High conductivities can be achieved at a high concentration if ionic mobilities are well maintained. Mole fraction normalized ionic conductivities were also calculated by normalizing the conductivity with respect to the mole fraction of LiTFSI (Figure 3.1.3.1).

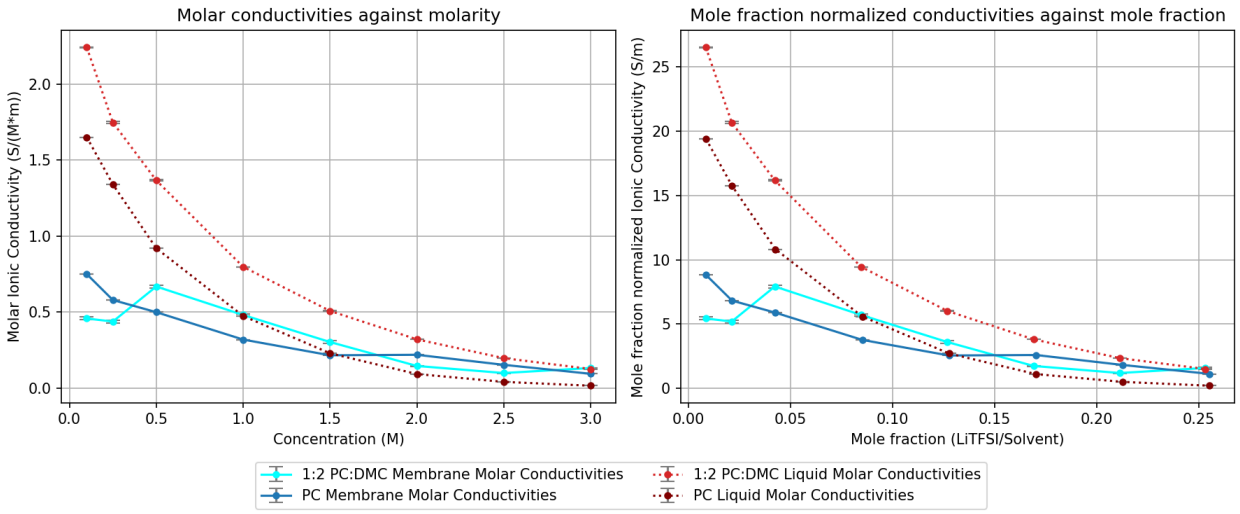

Figure 3.1.3.1: Molar conductivity and mole fraction normalized conductivities. The same colouring convention is maintained as with the conductivity plot. Liquid samples show similar relationships, with the addition of DMC into the solvent offering higher ionic mobility. Polymer samples lose mobility at high concentrations, but the effect is much less significant. Ionic mobilities converge between polymer and bulk PC:DMC samples at 3M.

The addition of DMC to the solvent mix results in a simple, across the board, enhancement in bulk solution ionic mobility. Neither type of membrane shows consistently higher ionic mobilities than the other, and both show mobilities that are more stable with concentration than

bulk solution. It may be possible for the membranes to achieve good mobilities at concentrations above 3M, but electrolyte saturation may prevent these from forming stable piezoionic sensors.

3.1.4 Accounting for "Interaction Sites"

Comparison between the different membranes has proved difficult, due in part to the differences in fabrication. Figuring out ion to solvent ratios in bulk electrolyte is trivial, but the existence of polymer interaction sites makes it much more challenging for the membrane samples. In an attempt to put all the ionic systems on an even playing field, one may choose to treat the polymer's interaction sites as lowering effective concentration, even if it technically cannot dissolve LiTFSI. [16] Conductivity and normalized conductivities were plotted against an estimated ratio of ions to "interaction sites" (Figure 3.1.4.1). For this analysis, it was assumed that PVDF-HFP consisted of equal parts PVDF and HFP, and that each monomer represents an additional solvent molecule, or "interaction site". The number of moles of PVDF monomers, HFP monomers, DMC, PC, and LiTFSI were estimated for the sample that was soaked and weighed afterward, accounting for the extra mass of electrolyte absorbed. The assumption was made that the amount of electrolyte absorbed into the membrane upon soaking would always be 24.23% of the membrane mass, based on the sample that was weighed before and after soaking. The moles of each species in a pure PC sample was calculated based on membrane composition, without any extra mass absorbed.

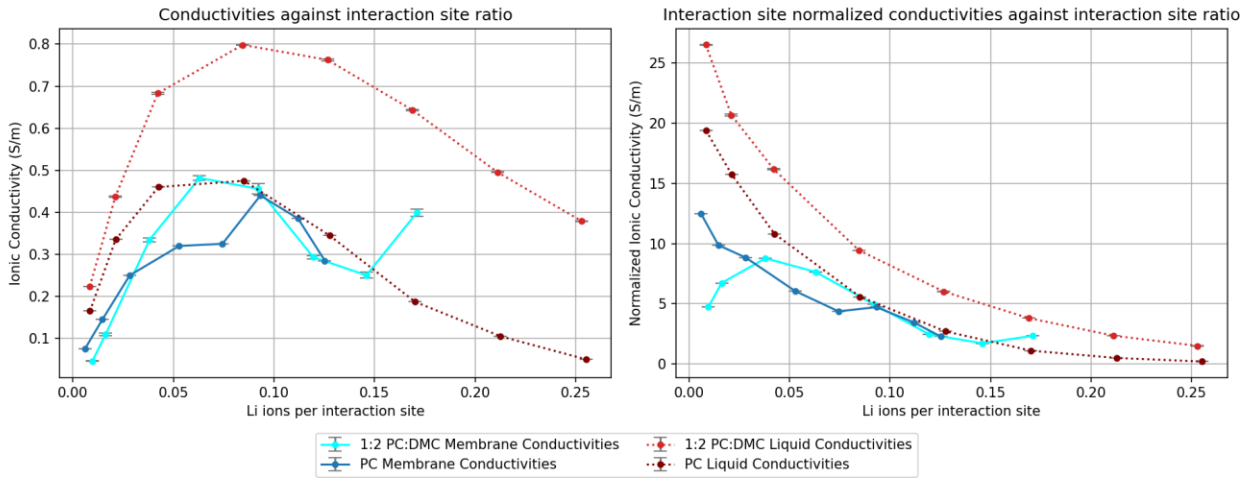

Figure 3.1.4.1: Ionic conductivity plotted against estimated interaction sites per mole of solute and normalized with respect to estimated interaction sites per mole of solute. While membrane conductivity changed rather slowly with respect to concentration, they change at rate similar to bulk solutions when compared with available interaction sites.

Considering the amount of ions per interaction site as the x-axis, the membrane ionic conductivity trends bear a closer resemblance to those observed in bulk solution. The PC:DMC/PVDF-HFP system shows somewhat similar conductivity across a similar x-axis range when compared with the bulk PC solution. Membrane samples transition from increasing to decreasing conductivity at a relatively similar number of interaction sites per solute, with the 3M PC:DMC membrane as an anomaly. A potential interpretation is that the electrolyte in the PVDF-HFP membranes can be thought of as being more dilute, due to the fact that the polymer provides stabilizing interactions similar to a solvent. Normalized with respect to interaction sites per ion, both membranes show similar or lower normalized conductivities than their bulk solution counterparts. If one normalizes conductivity with respect to Li ions per interaction site, one gets a similar metric to molar conductivity that considers the ionic system to be diluted by the polymer membrane. The normalized data paints a similar picture to the un-normalized data,

with the polymer membranes showing values that are comparable to those of the bulk PC electrolyte sample at the same level of dilution. This analysis must be taken with a grain of salt as fluorinated hydrocarbons do not technically solvate LiTFSI well, but they play a similar role by providing stabilizing interactions and may cause the fluid to behave more dilute. [16]

3.2 NMR Data Analysis

3.2.1 Diffusion Coefficient Data

Diffusion coefficients were measured for lithium ions in LiTFSI/PC:DMC and LiTFSI/PC:DMC/PVDF-HFP at 0.1M and 1.5M, and compared with results from Dobashi Et al (Figure 3.2.1.1).

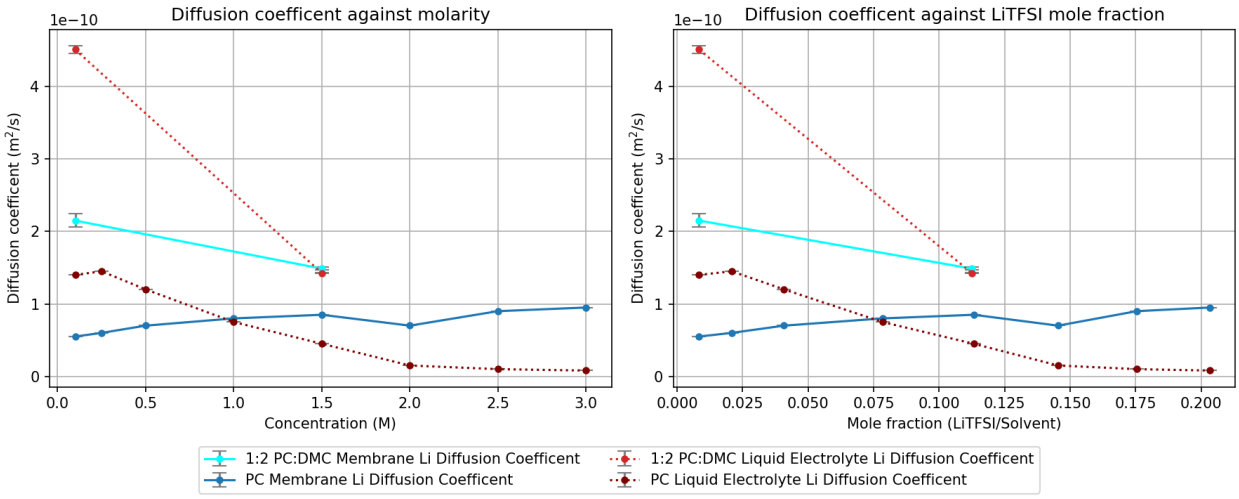

Figure 3.2.1.1: Lithium diffusion coefficients measured in 1:2 PC:DMC electrolyte systems, compared with data from Dobashi et al for PC electrolyte systems. The addition of DMC to the solvent mix appears to increase diffusion across the board, likely due to its lower viscosity. Bulk electrolyte values are understandable, and discrepancies with conductivity data are explainable through the contribution of TFSI to mobility. PC:DMC membrane diffusion coefficients are higher than ionic conductivity measurements would suggest, calling into question if the parameters of the PFG-NMR sequence were chosen correctly for the membranes under study. PC:DMC membrane diffusion also decreases with concentration, suggesting major changes in ionic atmosphere compared with PC membranes.

Bulk electrolyte diffusion coefficients mirror the trends in ionic conductivity, with fast diffusion across the board. From 0.1M to 1.5M, bulk PC:DMC molar conductivity decreases by a factor of about 4.5, while the lithium diffusion coefficient only decreases by a factor of about 3. Changes in lithium diffusion coefficients will not fully explain changes in molar conductivity, because TFSI might account for the majority of ionic mobility at low concentrations, similar to the data acquired by Dobashi et al and Petel.

The PC:DMC/PVDF-HFP samples show very high diffusion coefficients, which don't correspond well with ionic conductivity measurements. Despite the 0.1M LiTFSI/PC:DMC membrane showing lower ionic conductivity than the 0.1M LiTFSI/PC membrane, the lithium diffusion coefficient is over four times as high. Lower conductivity with a higher diffusion coefficient suggests either strong ion pairing or a very immobile TFSI ion. Neither explanation makes a lot of sense at low concentrations. The validity of this particular diffusion coefficient measurement is called into question given the fact that the gaussian curve fit for this data point appears noisy (Figure 3.2.1.2). A poor signal to noise ratio may have resulted from the low number of ions in the sample, and future measurements may be improved with greater signal averaging, a better resolution of gradient values, and by putting more sample into the NMR tube. Poor results may also be a product of multi-phase diffusion, which can be fit to data following a multi phase Stejskal and Tanner equation (Equation 3.2.1.1).

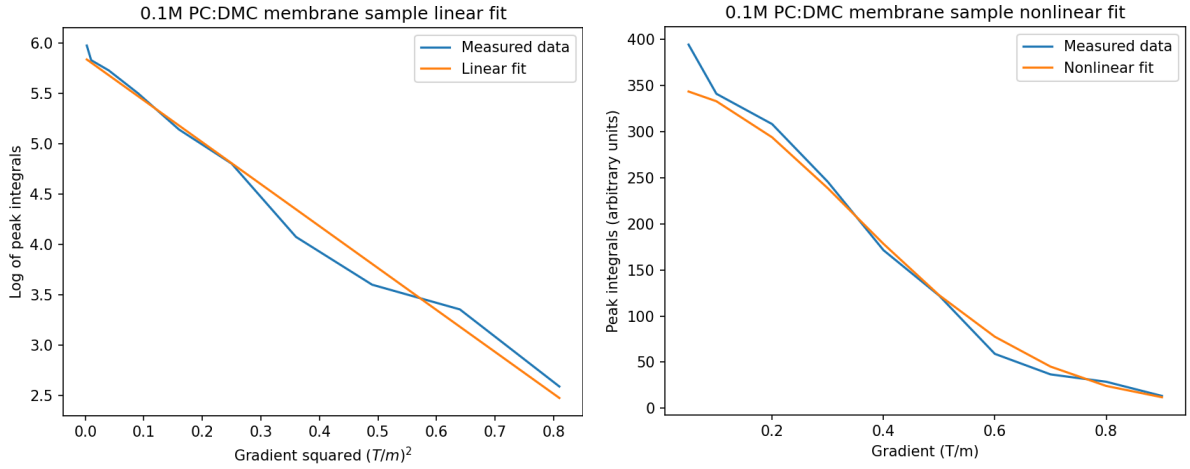

Figure 3.2.1.2: Linear and gaussian fits for the PFG-NMR data for the 0.1M PC:DMC membrane. Poor fit quality may be indicative of bad signal to noise ratio, or multi phase diffusion. Low gradient resolution prohibited a double gaussian curve fit. Detecting multi phase diffusion would require more data at high or low gradients to capture the contour of the other phase's response.

$$S = S_0\left(f_{slow} exp\left(-D_{slow}\gamma^2\ \delta^2\ g^2\ \left(\Delta - \frac{\delta}{3}\right)\right) + f_{fast} exp\left(-D_{fast}\gamma^2\ \delta^2\ g^2\ \left(\Delta - \frac{\delta}{3}\right)\right)\right)$$ EQ 3.2.1.1

D_{slow}, D_{fast} are the two diffusion coefficients and f_{slow}, f_{fast} are their relative abundances in the sample. A secondary phase of diffusion may be a slower polymer phase, which would only show up at high gradient strengths, but this is unlikley as Li ions do not have a strong affinity for the PVDF-HFP membranes. [16], [17] A second, faster, phase of diffusion may be due to liquid electrolyte stuck to the outside of the polymer with surface tension. Excess liquid electrolyte was mitigated by tipping out the NMR tube onto filter paper to absorb any electrolyte that dripped out, leaving the soaked polymer inside, but some may remain due to surface tension. A liquid diffusion phase would show up as another gaussian shape at low gradient values, that would decay before the main polymer phase's response. Some irregularities can be made out at low gradients, but resolution is limited by poor gradient resolution and noisy data.

Despite lower molar conductivity, the 1.5M PC:DMC membrane also shows an anomalously high diffusion coefficient, similar to that of 1.5M PC:DMC bulk electrolyte. The quality of the gaussian curve fit is quite good, owing to the concentrated sample providing a strong response with good signal to noise ratio. If there was multi phase diffusion from liquid on the surface, it would be impossible to tell because the polymer and liquid have the same Li diffusion coefficient. A more likely explanation for the anomalously high diffusion coefficient is restricted diffusion. PFG-NMR measures how far ions move through Brownian motion in a time Δ, and relates it to the diffusion coefficient which can be related through Equation 3.2.1.2. All PFG-NMR measurements were performed with a small diffusion time of 0.2s, meaning that diffusion lengths varied from 6μm to 9μm. NMR measurements performed by Dobashi et al and

Petel used diffusion times varying from 0.45s to 0.9s which, for the diffusion coefficients measured in PC:DMC, mean diffusion lengths varying from 9.48μm to 13.41μm.

$$L_d \approx \sqrt{D\Delta} \text{ EQ 3.2.1.2}$$

If an ion's movement is restricted by pore size, once $\sqrt{D\Delta}$ exceeds the pore size, PFG-NMR will measure smaller diffusion length due to collisions with the pore walls, and the effective diffusion coefficient that is measured will be smaller. Hinderance from pores may reduce ionic conductivity, but will not show up in NMR measurement unless the diffusion time is chosen for ions to hit those pore walls. A possible explanation for PC:DMC membrane samples showing high diffusion coefficient as compared to molar conductivity is that restrictions in ion motion, due to pore sizes larger than 9μm, were not measured. Such hindrance effects from the polymer matrix may be better accounted for by performing PFG-NMR with a variety of diffusion times, to attempt to probe the pore size in the membrane

The reduction in diffusion coefficient with concentration in the PC:DMC swollen membrane indicates substantial differences in ionic atmosphere, compared with the PC swollen membrane. Whatever interaction caused ion pairing to reduce with concentration in the PC membranes is not occurring with the PC:DMC solvent mix. The greater miscibility of DMC with the polymer backbone may also explain differences, as pore structure, or interactions with the PVDF-HFP interaction sites could be modified. If DMC solvates PVDF-HFP and blocks TFSI interaction sites, the ionic environment in the pores would be more like that of bulk electrolyte, with ion pairing increasing with concentration. The 3M PC:DMC membrane shows a sudden turnaround in ionic conductivity/mobility, and has promise for piezoionic sensors due to its high

ionic conductivity. The 3M membrane sample would be a logical next step for further diffusion measurements. Anion diffusion measurements would allow estimations of conductivity with the Nernst-Einstein equation (Equation 1.2.1.2) and estimates of ion pairing.

3.2.2 T1 Relaxation Data

T1 relaxation times were acquired and analyzed for 0.1M and 1.5M PC:DMC systems (Figure 3.2.2.1).

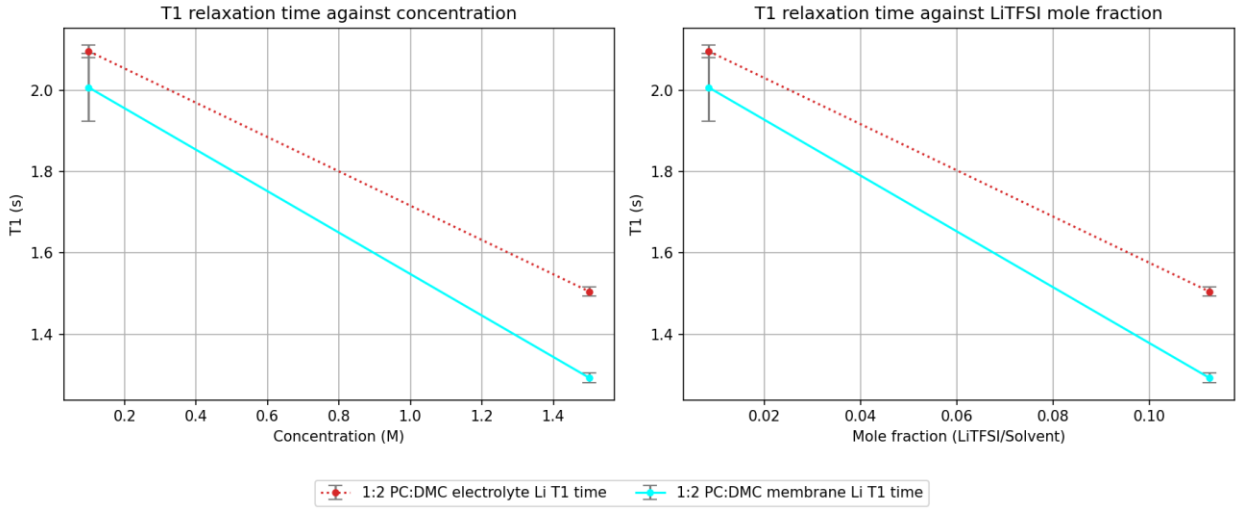

Figure 3.2.2.1: Relaxation times against concentration and mole fractions. All values are within a factor 2 of one another, indicating similar ionic atmospheres. T1 times decrease with concentration due to a combination of greater solvent viscosity and increased ion pairing. Bulk electrolyte shows higher T1 decay times, suggesting fast tumbling movement of ions compared with the polymer.

T1 decay times corroborate conductivity and diffusion measurements well, indicating that ions in bulk solution are faster tumbling compared to ions in the polymer. T1 relaxation times being on a similar order to one another suggest a similar solvation environment, without lithium ions being held in any kind of solid-state polymer diffusion phase. The large uncertainty in the 0.1M PC:DMC membrane T1 is indicative of poor signal to noise ratio, owing to the small amount of lithium in the sample and weak signal. The subtle reduction in T1 values across concentration is

characteristic of a more viscous ionic atmosphere, or ion pairing, and occurs in both bulk and membrane systems. Membrane T1 values are consistently lower than bulk electrolyte values, suggesting the ions are generally tumbling more slowly. Despite having the same diffusion coefficients, the 1.5M membrane shows a lower T1 as compared with the bulk solution. The 1.5M membrane also shows lower conductivity than the bulk solution, so it may be possible that there is a greater degree of ion pairing inside the PVDF-HFP membrane, lowering T1 and conductivity while allowing the diffusion coefficient to remain high. Such ion pairing may be investigated by looking for TFSI diffusion coefficients similar to those of Lithium. Increased ion pairing at 1.5M would suggest that the addition of DMC prevents the PVDF-HFP from interacting with TFSI, preventing it from shielding the lithium against ion pairing.

Chapter 4: Conclusions and Future Direction

The use of thinner solvents shows promise for enhancing the piezoionic effect in PVDF-HFP, but dimethyl carbonate does not appear to be the ideal candidate. The bulk PC:DMC solvent mix showed all the ionic properties one would want for a piezoionic electrolyte, offering high diffusion coefficients and mobility, likely due to low viscosity. The conductivity trends in the membranes were difficult to explain, and conductivity was not necessarily enhanced. A further study should investigate mobility of TFSI ions to determine how they are contributing to the overall conductivity. Looking for similar anion and cation diffusion coefficients, as well as comparing measured ionic conductivities against NMR based estimates will shed more light on the degree and nature of ion pairing in these complex membrane systems. The 3M membranes are of interest, due to very high conductivity at high concentrations, and represent a distinct regime where the PC:DMC membranes may surpass the piezoionic performance of Dobashi et al's membranes.

Adding dimethyl carbonate to the solvent mix appears to enhance diffusion coefficients in membranes, but ionic conductivity measurements do not reflect high mobilities. Further NMR spectroscopy, using longer diffusion times, should be performed to probe pore size and whether restricted diffusion is occurring. While unlikely, high resolution NMR spectroscopy may also reveal multi-phase diffusion. Membranes with DMC show diffusion coefficients that decrease with concentration, indicating that ion pairing may not be suppressed the way it is in Dobashi et al's membranes. T1 measurements also suggest the possibility of ion pairing, explaining why high diffusion coefficients do not correspond with high mobility.

Despite showing some promising ionic properties, dimethyl carbonate may be an unwise choice for a co-solvent in a piezoionic sensor. Dimethyl carbonate appeared to dissolve membranes, reducing their strength and stretchability, transforming them from a relatively robust elastomer to a softer more gel-like elastomer. Lithium diffusion coefficients appeared to decrease with concentration in membranes with the binary solvent mix, indicating that DMC may induce changes to the membrane structure that enhance ion pairing. The most significant downside of dimethyl carbonate is owed to its volatility, requiring changes to Dobashi et al's fabrication procedure. Membranes with DMC cannot be left out for more than a few minutes without drying out, making any rheological characterization extremely difficult. For the goals of developing more sensitive piezoionic sensors, future work should investigate the possibility of a less volatile thinning agent, and one that has a lower miscibility in PVDF-HFP. Another good option for future work is studying encapsulation methods that can prevent solvent evaporation from these membranes. Packaging techniques will also need to be developed for LiTFSI PVDF-HFP piezoionic sensors to mitigate toxicity and make them biocompatible.

Bibliography

[1] Woehling, Vincent, Giao T M Nguyen, Cedric Plesse, Yael Petel, Yuta Dobashi, John D W Madden, Carl A Michal, and Frederic Vidal. "Study of the Piezoionic Effect and Influence of Electrolyte in Conducting Polymer Based Soft Strain Sensors." *Multifunctional Materials* 2, no. 4 (December 2019): 045002. https://doi.org/10.1088/2399-7532/ab56a2.

[2] Dobashi, Yuta, Dickson Yao, Yael Petel, Tan Ngoc Nguyen, Mirza Saquib Sarwar, Yacine Thabet, Cliff L. W. Ng, et al. "Piezoionic Mechanoreceptors: Force-Induced Current Generation in Hydrogels." *Science* 376, no. 6592 (April 29, 2022): 502–7. https://doi.org/10.1126/science.aaw1974.

[3] Petel, Yael. "Transport in Ion Dense Media and Recyclable Polymers." University of British Columbia, 2020. https://doi.org/10.14288/1.0392849.

[4] Cai, Ming, Ding Yuan, Xiao Zhang, Yi Pu, Xiaofang Liu, Hongwei He, Lixue Zhang, and Xin Ning. "Lithium Ion Battery Separator with Improved Performance via Side-by-Side Bicomponent Electrospinning of PVDF-HFP/PI Followed by 3D Thermal Crosslinking." *Journal of Power Sources* 461 (June 15, 2020): 228123. https://doi.org/10.1016/j.jpowsour.2020.228123.

[5] Pu, Weihua, Xiangming He, Li Wang, Changyin Jiang, and Chunrong Wan. "Preparation of PVDF–HFP Microporous Membrane for Li-Ion Batteries by Phase Inversion." *Journal of Membrane Science* 272, no. 1 (March 15, 2006): 11–14. https://doi.org/10.1016/j.memsci.2005.12.038.

[6] Hogen-Esch, T. E., and J. Smid. "Solvent-Separated Ion Pairs of Carbanions." *Journal of the American Chemical Society* 87, no. 3 (February 1, 1965): 669–70. https://doi.org/10.1021/ja01081a059.

[7] Seo, Daniel M., Stefanie Reininger, Mary Kutcher, Kaitlin Redmond, William B. Euler, and Brett L. Lucht. "Role of Mixed Solvation and Ion Pairing in the Solution Structure of Lithium Ion Battery Electrolytes." *The Journal of Physical Chemistry C* 119, no. 25 (June 25, 2015): 14038–46. https://doi.org/10.1021/acs.jpcc.5b03694.

[8] "Ethylene Carbonate." Accessed May 3, 2025. https://www.stenutz.eu/chem/solv6.php?name=ethylene+carbonate.

[9] Ponrouch, Alexandre, Elena Marchante, Matthieu Courty, Jean-Marie Tarascon, and M. Rosa Palacín. "In Search of an Optimized Electrolyte for Na-Ion Batteries." *Energy & Environmental Science* 5, no. 9 (August 15, 2012): 8572–83. https://doi.org/10.1039/C2EE22258B.

[10] Ponnuchamy, Veerapandian, Stefano Mossa, and Ioannis Skarmoutsos. "Solvent and Salt Effect on Lithium Ion Solvation and Contact Ion Pair Formation in Organic Carbonates: A Quantum Chemical Perspective." *The Journal of Physical Chemistry C* 122, no. 45 (November 15, 2018): 25930–39. https://doi.org/10.1021/acs.jpcc.8b09892.

[11] “Investigation of Dimethyl Carbonate and Propylene Carbonate Mixtures for LiNi0.6Mn0.2Co0.2O2-Li4Ti5O12 Cells | Request PDF.” *ResearchGate*, December 9, 2024. https://doi.org/10.1002/celc.201900672.

[12] Agatha, Edimeh, C. Grace, M. Jane, and Abia Augustine. “Conductivity and Viscosity Studies of Binary Mixtures of Dimethyl Carbonate and Dimethyl Sulphoxide Based Electrolyte for Li-Ion Battery at 298 . 15 k,” 2017. https://www.semanticscholar.org/paper/Conductivity-and-Viscosity-Studies-of-Binary-of-and-Agatha-Grace/5d2c33e434478c71a9cdaa8edbc5b846d19b875a.

[13] Fujii, Kenta, Takao Fujimori, Toshiyuki Takamuku, Ryo Kanzaki, Yasuhiro Umebayashi, and Shin-Ichi Ishiguro. “Conformational Equilibrium of Bis(Trifluoromethanesulfonyl) Imide Anion of a Room-Temperature Ionic Liquid: Raman Spectroscopic Study and DFT Calculations.” *The Journal of Physical Chemistry. B* 110, no. 16 (April 27, 2006): 8179–83. https://doi.org/10.1021/jp0612477.

[14] Bhatt, Mahesh Datt, Maenghyo Cho, and Kyeongjae Cho. “Conduction of Li+ Cations in Ethylene Carbonate (EC) and Propylene Carbonate (PC): Comparative Studies Using Density Functional Theory.” *Journal of Solid State Electrochemistry* 16, no. 2 (February 1, 2012): 435–41. https://doi.org/10.1007/s10008-011-1350-7.

[15] Shi, P. C., M. Lin, H. Zheng, X. D. He, Z. M. Xue, H. F. Xiang, and C. H. Chen. “Effect of Propylene Carbonate-Li+ Solvation Structures on Graphite Exfoliation and Its Application in Li-Ion Batteries.” *Electrochimica Acta* 247 (September 1, 2017): 12–18. https://doi.org/10.1016/j.electacta.2017.06.174.

[16] Hernández, Guiomar, Tian Khoon Lee, Máté Erdélyi, Daniel Brandell, and Jonas Mindemark. “Do Non-Coordinating Polymers Function as Host Materials for Solid Polymer Electrolytes? The Case of PVdF-HFP.” *Journal of Materials Chemistry A* 11, no. 28 (July 18, 2023): 15329–35. https://doi.org/10.1039/D3TA01853A.

[17] Jie, Jing, Yulong Liu, Lina Cong, Bohao Zhang, Wei Lu, Xinming Zhang, Jun Liu, Haiming Xie, and Liqun Sun. “High-Performance PVDF-HFP Based Gel Polymer Electrolyte with a Safe Solvent in Li Metal Polymer Battery.” *Journal of Energy Chemistry* 49 (October 1, 2020): 80–88. https://doi.org/10.1016/j.jechem.2020.01.019.

[18] Richardson, Peter Michael. “NMR Studies of Ionic Mobility in PVDF Based Polymer Gel Electrolytes.” Phd, University of Leeds, 2013. https://etheses.whiterose.ac.uk/id/eprint/6452/.

[19] Oldham, Keith B., and Nicholas P. C. Stevens. “Uncompensated Resistance. 2. The Effect of Reference Electrode Nonideality.” *Analytical Chemistry* 72, no. 17 (September 1, 2000): 3981–88. https://doi.org/10.1021/ac000154x.

[20] Purkait, Mihir Kumar, Manish Kumar Sinha, Piyal Mondal, and Randeep Singh. “Chapter 1 - Introduction to Membranes.” In *Interface Science and Technology*, edited by Mihir Kumar Purkait, Manish Kumar Sinha, Piyal Mondal, and Randeep Singh, 25:1–37. Stimuli Responsive Polymeric Membranes. Elsevier, 2018. https://doi.org/10.1016/B978-0-12-813961-5.00001-2.

[21] Michan, Alison Louise. “Nuclear Magnetic Resonance Characterization of Solid Polymer Electrolyte Materials.” University of British Columbia, 2012. https://doi.org/10.14288/1.0072863.

[22] Xin, Nan, Yanjun Sun, Maogang He, Clayton J. Radke, and John M. Prausnitz. “Solubilities of Six Lithium Salts in Five Non-Aqueous Solvents and in a Few of Their Binary Mixtures.” *Fluid Phase Equilibria* 461 (April 15, 2018): 1–7. https://doi.org/10.1016/j.fluid.2017.12.034.

[23] Kim, Jung Yong. “Phase Behavior of Binary and Ternary Fluoropolymer (PVDF-HFP) Solutions for Single-Ion Conductors.” *RSC Advances* 12, no. 33 (July 21, 2022): 21160–71. https://doi.org/10.1039/D2RA04158H.

[24] “The Stejskal–Tanner Equation Generalized for Any Gradient Shape—an Overview of Most Pulse Sequences Measuring Free Diffusion.” Accessed May 3, 2025. https://doi.org/10.1002/cmr.a.21223.

[25] Tanner, J. E. “Use of the Stimulated Echo in NMR Diffusion Studies.” *The Journal of Chemical Physics* 52, no. 5 (March 1, 1970): 2523–26. https://doi.org/10.1063/1.1673336.

Appendix A NMR spectroscopy

A.1 NMR Basics

In NMR spectroscopy, a strong magnetic field B_Z is placed over the sample, causing spins to settle parallel to the field. An RF pulse is applied to rotate the net spin magnetization vector 90°, perpendicular to the field, which will cause Larmour precession at the frequency $\omega_L = \gamma B_z$ where γ is the gyromagnetic ratio of the nucleus being targeted. An RF signal at the Larmour frequency can be measured so long as spins across the sample are in phase. If the real and imaginary components represent x and y components, the spin magnetization vector density of a tiny section of the sample at a given time can be represented with the following equation.

$$S(t) = S_0 e^{-i\omega_z t} * e^{-\frac{t}{T_2}} \quad \text{EQ A1}$$

T_2 represents the time constant for spin-spin relaxation, a natural form of decay that occurs when spins are precessing, and S_0 represents the magnitude of the signal strength immediately after the 90° pulse is delivered.

A.2 Spin Echo

All NMR probe fields have a very subtle gradient in their field profile. Assuming a linear 1-dimensional gradient as a simple example, the field profile is given as $B_z + z * g_0$ where g_0 is the magnetic field gradient given in Teslas per Meter. The Larmour frequency will be modified in a spatially dependent manner as $\omega_L = \gamma(B_z + z * g_0)$ and spins in any two locations z_1, z_2 will have a frequency difference of $\Delta\omega_L = \gamma g(z_1 - z_2)$. Spins across the sample will lose phase coherence over time with a phase difference of $\Delta\phi = \gamma g(z_1 - z_2)t$. The spin magnetization density over time at each location can be expressed as

$$S(t,z) = S_0 e^{-i\gamma B_z t} * e^{-i\gamma g_0 z t} e^{-\frac{t}{T_2}} \text{ EQ A2}$$

The first term represents the precession that occurs as a result of the ideal uniform field, identical in every part of the sample. It is customary to ignore this component by considering a rotating reference frame, spinning at the frequency that would be seen with no gradient. In the rotating reference frame, the spin magnetization density is given as

$$S(t,z) = S_0 e^{-i\gamma g_0 z t} e^{-\frac{t}{T_2}} \text{ EQ A3}$$

The NMR signal strength will be proportional to the net spin magnetization vector, which is given by an integral across z. The overall signal will weaken as spins at different values of z go out of phase and begin cancelling one another out. This initial weakening of the signal is called the free induction decay (FID) If one applies an RF pulse to shift all phases by 180°, it will effectively put a negative sign on all the phase that has been accrued in each section of the

sample. If a 180° pulse is applied at time τ, the spin magnetization density vector in the rotating reference frame will be given by.

$$S(t,z) = S_0 * e^{i\gamma g_0 z\tau} * e^{-i\gamma g_0 z(t-\tau)} * e^{-\frac{t}{T_2}} \text{ EQ A4}$$

If one waits for another τ after the 180° pulse ($t = 2\tau$), the accrued phases will cancel out leaving all spins at their original orientation.

$$S(2\tau,z) = S_0 * e^{i\gamma g_0 z\tau} * e^{-i\gamma g_0 z\tau} * e^{-\frac{2\tau}{T_2}} = S_0 * e^{-\frac{2\tau}{T_2}} \text{ EQ A5}$$

With the spatial dependence of phase gone, the spins at all locations are all pointing at the same direction at $t = 2\tau$, and the measured signal strength will reach a maximum called an echo. In practice, it is quite hard to measure FID, so NMR measurement is typically done by measuring echoes.

A.3 Pulsed Gradient Sequences

A strong gradient pulse, $g \gg g_0$, that lasts for a finite duration δ, will encode a spatially dependent phase difference between two points on the sample given as $\Delta\phi = \gamma g \delta (z_1 - z_2)$. After a short strong gradient pulse, spin magnetization density in a rotating frame can be represented as

$$S(t,z) = S_0 e^{-iz\gamma g_0 t} e^{-iz\gamma g \delta} * e^{-\frac{t}{T_2}} \quad \text{EQ A6}$$

If one would like to cancel out the phases accrued from the gradients, one can apply a 180° pulse at time τ onto the signal and then apply the same gradient pulse afterward. Assuming the spin of interest does not move, the gradient pulse phases will cancel and spin magnetization density will be given by

$$S_0 e^{iz\gamma g_0 \tau} * e^{-iz\gamma g_0 (t-\tau)} * e^{-\frac{t}{T_2}} \quad \text{EQ A7}$$

At $t = 2\tau$ the echo will occur. Due to the very high value of g, the pulsed gradient component of the phase is extremely sensitive to movement of the spin carrying particles, such as Brownian motion of ions in solution. If an ion moved from position $z(t_{g1})$ at the time of the first gradient pulse to $z(t_{g2})$ at the time of the second gradient pulse, the spin magnetization density at the echo time will be equal to.

$$S(2\tau,z) = S_0 e^{-i\left(z(t_{g1}) - z(t_{g2})\right)\gamma g \delta} * e^{-\frac{2\tau}{T_2}} \quad \text{EQ A8}$$

The greater the amount of ion movement, the greater the dephasing at the echo time, and the weaker the echo. Pulsed field gradient NMR can take advantage of the relationship between Brownian motion and echo strength to calculate the diffusion coefficient of ions in solution.

Measurements were conducted using a modified version of the famous Stejskal and Tanner pulse sequence (Figure A1).

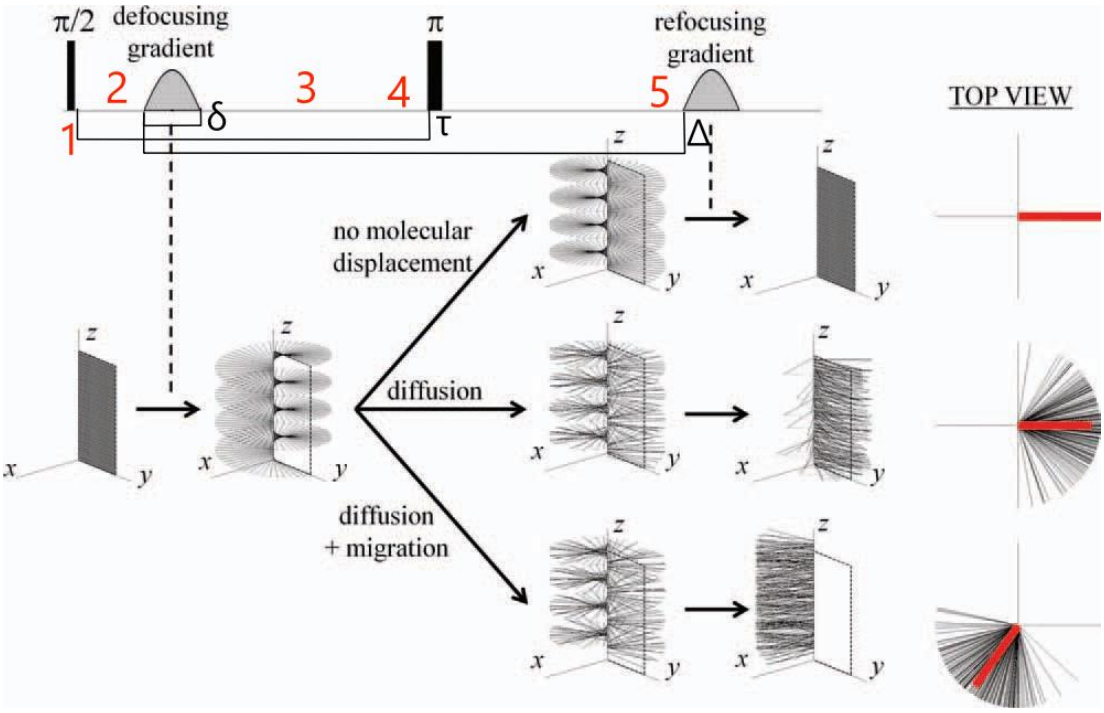

Figure A1: the Stejskal and Tanner sequence, adapted from [24]. Time labels are added, τ represents the time between the 90° and 180° pulses, δ represents the duration of the gradient pulse, and Δ represents the time between the two gradient pulses, or the diffusion time.

1: an RF pulse rotates the spin magnetization vector in each location of the sample by 90 deg, causing spins to precess about the Z axis at their Larmour frequency.

2: A gradient pulse will be applied, spin magnetization in each part of the sample receives a phase shift that is dependent on its position, causing a position encoding dephasing across the length of the sample.

3: Ions are given time to diffuse, maintaining the position dependent phase shift that they accrued from the gradient pulse.

4: An RF pulse shifts all spin phases by 180°, effectively applying a negative sign to the accrued phase. If spins can accrue the exact opposite phase that they accrued before the 180° pulse, they will rephase at the same time creating a detectible RF signal called an “echo”.

5: An identical gradient pulse will attempt to rephase the spins inside the sample. Ions have moved to different parts of the sample and will accrue a different phase shift from the same gradient pulse. A greater amount of diffusion results in a greater difference in ion position, and a weaker echo.

Creating a simple mathematical expression for the received signal intensity requires the assumption that the static gradients are negligible compared to the pulsed gradients. [25] Field inhomogeneities in modern NMR probes, such as the one used for this experiment, are negligible and can thus be ignored. [21] The intensity of the received echo $S_{2\tau}$ after performing the Stejskal and Tanner sequence with a square gradient pulse is given by.

$$S_{2\tau} = S_0 \exp\left(-D\gamma^2\delta^2 g^2\left(\Delta - \frac{\delta}{3}\right)\right) * \exp\left(\frac{2\tau}{T_2}\right) \text{EQA9}$$

Where S_0 represents the signal strength that would be measured immediately after the first pulse is applied, D is the diffusion coefficient of the nucleus being studied, δ is the duration of the gradient pulse, g is the strength of the gradient pulse in Teslas per Metre, Δ is the diffusion time, and τ is the time between the 90° and 180° pulses. In practice S_0 is difficult to measure, so it is customary to normalize things with respect to the signal intensity that would be seen with no gradient, getting the Stejskal and Tanner equation.

$$\ln\left(\frac{S}{S_{no\ gradient}}\right) = -D\gamma^2\delta^2 g^2\left(\Delta - \frac{\delta}{3}\right) \text{EQ A10}$$

A.4 Stimulated Echo

The original Stejskal and Tanner pulse sequence fails in the case of viscous liquids, like electrolytes, because of their fast T2 decay time. A modified version of the original ST sequence is used for this experiment. The first modification is a technique called stimulated echo. Instead

of using a 180°, a second 90° pulse is used to “store” the phase of the rotating spins. A component of the spin magnetization vector at each point will end up parallel or antiparallel to the magnetic field, and this component of spin encodes phase. The stored spin magnetization will undergo T1 decay, also called spin lattice relaxation, but not T2 decay. Stored spins will maintain their gradient based phase encoding until another 90° pulse sets them back in motion in the transverse plane, beginning the rephasing part of the pulse sequence. The storage part of the NMR sequence allows for very long diffusion times to be used and makes the technique able to measure smaller diffusion coefficients as well as samples with low T2. [25]

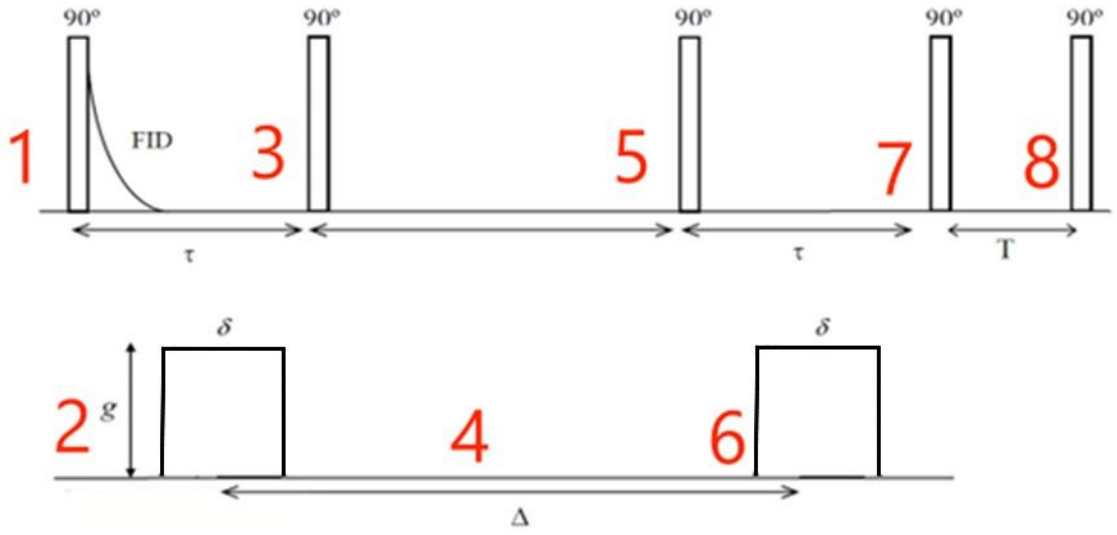

Figure A2, adapted from Dobashi et al [2]. Credit to Elizabeth Lim for edits

Diagram of the pulsed gradient stimulated echo sequence used.

1: Initial 90° excitation pulse causes spins to begin precessing

2: A short strong gradient pulse encodes ion positions in the accrued phase from the pulse

3: Another 90° pulse stores the spin phase in parallel and antiparallel components to the static magnetic field

4: Ions are allowed to diffuse for the diffusion time Δ, shielded from T2 decay, but experiencing T1 decay which is typically slower

5: After the diffusion time is up, a 90° pulse flips the spins again to begin the refocusing process

6: A copy of the original gradient is applied, with the degree of refocusing relating to how far the ions have diffused

7: The spins are stored once again with a 90° pulse, immediately at the echo time. The spins will be stored for a time T to allow eddy currents from the last gradient pulse to decay, improving signal to noise ratio

8: The spins are put back into motion with another 90° pulse and the signal is acquired

The strength of the echo after the PFG NMR sequence can be given by

$$S(2\tau) = S_0 \frac{1}{4} \exp\left(-D\gamma^2\delta^2 g^2 \left(\Delta - \frac{\delta}{3}\right)\right) e^{-\frac{2\tau}{T_2}} e^{-\frac{\Delta-\tau}{T_1}} \quad \text{EQ A11}$$

Where S_0 represents the strength of the signal that would be measured immediately after the excitation. The factor 4 loss comes from the 2 storage sequences, the first exponential represents loss from the diffusion dependant dephasing from the gradient pulses, the second exponential represents T2 decay outside the diffusion time, and the third exponential represents T1 decay during the diffusion time. Normalizing with respect to the signal without a gradient pulse removes the factor 4 loss, and removes T1 and T2 decays, getting the Stejskal and Tanner equation once again.

$$\ln\left(\frac{S}{S_{no\ gradient}}\right) = -D\gamma^2\delta^2 g^2\left(\Delta - \frac{\delta}{3}\right) \text{ EQ A10}$$

A.5 Acquiring Diffusion Coefficients with PFG-STE NMR

$$\ln(S) = \ln\left(S_{no\ gradient}\right) - D\gamma^2\delta^2 g^2\left(\Delta - \frac{\delta}{3}\right) \text{ EQ A10}$$

One can acquire the diffusion coefficient of the sample by curve fitting equation A10, varying either the gradient pulse length δ, the diffusion time Δ, or the gradient strength g. Varying Δ is problematic as different sequences will experience different amounts of T1 decay and samples must be normalized relative to this to fit the ST equation. Varying δ is problematic due to the somewhat convoluted dependence of the signal on δ. For measuring the diffusion coefficient of lithium, it was chosen to vary the gradient strength g, and a linear plot of ln (S) against g^2 was curvefit. The slope represents $-D\gamma_{Li^7}^2\left(\Delta - \frac{\delta}{3}\right)$ which can be used to acquire the diffusion coefficients. The y intercept represents ln ($S_{no\ gradient}$) which is an unpredictable and fairly

arbitrary function of the sample, test setup, and pulse sequence. If a clean single diffusion constant fit is achieved, it indicates that the ion being studied exists in only one kind of ionic environment. [3]